Fall 2016

Accurate imepdance measurement of O clip and near field coupling estimation using equivalent dipole moment model

Qiaolei Huang

Department:

ACCURATE IMPEDANCE MEASUREMENT OF O CLIP AND NEAR FIELD COUPLING ESTIMATION USING EQUIVALENT DIPOLE MOMENT MODEL

by

QIAOLEI HUANG

A THESIS

Presented to the Faculty of the Graduate School of the

MISSOURI UNIVERSITY OF SCIENCE AND TECHNOLOGY

In Partial Fulfillment of the Requirements for the Degree

MASTER OF SCIENCE IN ELECTRIC ENGINEERING

2016

Approved by

Dr. Jun Fan, Advisor
Dr. David Pommerenke
Dr. Daryl Beetner

ABSTRACT

As cellphones and electronic devices moves towards higher date rates yet smaller form factor, designer face more electromagnetic interference (EMI) and radio frequency interference (RFI)problems. In order to better guide the early design; designers want to know the exact electrical performance of small components, coupling estimation between components.

In Section 1, a de-embedding method is proposed to measure the impedance of an innovative O-shape spring contact, for frequency up to 30 GHz. The measurements are performed under the same condition when it's actually used in cellphones. De-embedding method will be applied to remove the fixture effects of the measurement setup, hence only the electrical performance of the DUT is obtained.

In Section 2, a dipole moment model is studied to investigate the near field RF coupling. A set of dipoles (both electric dipoles and magnetic dipoles) will be used to fit the measured tangential H field of the near field scanning. The dipoles will be built in 3D simulation tool. Together with the nearby antenna, the coupling between the dipole source and the victim antenna can be obtained. This dipole moment method is verified by both measurement and direct simulation data.

ACKNOWLEDGMENTS

I would like to express my great gratitude to my advisor, Dr. Jun Fan, for his guidance, encouragement, and trust throughout my master study. I learned a lot from him not only at the technical side, but also the non-technical side. He helped me gain a big picture of how to deal with research work, the people around, and also family. I feel fortunate to work with him and be his student.

I would also like to thank Dr. Drewniak, who guided me how to be a mature and responsible man. I learned a lot from him too. I would like to thank Dr. David Pommerenke , Dr. Beetner and Dr. Victor Khilkevich for their advice and help on my research work.

I also feel grateful to Yansheng Wang, Guangyao Shen, Xiangyang Jiao, Xiao Li, Xiang Fang, Liang Li, Jing Li. Every one of them helped me a lot in my research and life in Rolla. Also my thanks go to all of the other faculty members and my fellow lab mates in the EMC group of Missouri S&T. I am happy to work with you.

I am deeply grateful to my family, including my girlfriend, Yuan. Thanks for their understanding and love all the time.

Finally, my sincere appreciation goes to my mother. I dedicate this thesis to her.

TABLE OF CONTENTS

Page

LIST OF ILLUSTRATIONS

Page

1. INTRODUCTION

As cellphones and electronic devices moves towards higher date rates yet smaller form factor, designer face more electromagnetic interference (EMI) and radio frequency interference (RFI)problems. In order to better guide the early design; designers want to know the exact electrical performance of small components, coupling estimation between components.

In order to achieve better mechanical and RF performance, an innovative O-shape spring contact (O-Clip), which is more commonly used in mobile device applications, is designed [1]. A de-embedding method is proposed to measure the impedance of an innovative O-shape spring contact, for frequency up to 30 GHz. The measurements are performed under the same condition when it's actually used in cellphones. De-embedding method will be applied to remove the fixture effects of the measurement setup, hence only the electrical performance of the DUT is obtained.

Noise coupling from IC to antenna is also a big challenge in cellphone industry. A dipole moment model is studied to investigate the near field RF coupling. A set of dipoles (both electric dipoles and magnetic dipoles) will be used to fit the measured tangential H field of the near field scanning. The dipoles will be built in 3D simulation tool. Together with the nearby antenna, the coupling between the dipole source and the victim antenna can be obtained. This dipole moment method is verified by both measurement and direct simulation data.

2. DE-EMBEDDING METHOD TO ACCURATELY MEASURE HIGH-FREQUENCY IMPEDANCE OF O SHAPE SPRING CONTACT

Spring contacts are usually assembled onto printed circuit boards (PCBs) to act as an electrical connection between two circuits or two PCBs. In order to achieve better mechanical and RF performance, an innovative O-shape spring contact (O-Clip), which is more commonly used in mobile device applications, is designed [1]. A typical O-shape spring contact is shown in Figure 2.1.

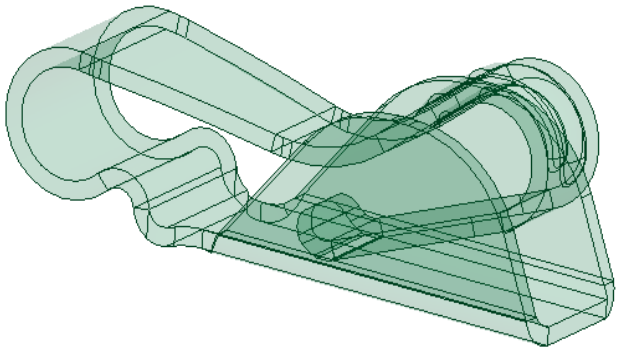

Figure 2.1. O shape spring contact (O Clip)

Compared with conventional spring contacts, such as pogo pins, and C-shape spring contacts, the O-Clip spring contacts have several advantages: lower cost, reduced size, and better RF performance especially at high frequencies. When the O-Clip is used as a board-to-board connection, it introduces smaller impedance to the electrical system due to the dual-path design than the conventional designs.

An accurate impedance measurement of the O-Clip needs to be performed at high frequencies. Currently, very small surface mount capacitance can be measured by specific RF impedance analyzer at frequencies from 1 MHz to 2.8 GHz [2]. However, for

the 3mm by 1mm by 1mm O-Clip connector, the impedance cannot be measured all the way up to 30 GHz, since at such high frequencies; the current distribution within the O-Clip significantly affects the impedance of the O-Clip. With different setups, different impedances will be measured due to different current distributions. Since O-Clips are mostly used as board-to-board connections, there are two current paths from the peak point to the ground plane of the O-Clip.

A de-embedding method to measure the impedance of the O-Clip is described below. As shown in Figure 2.2, two PCBs of equal size are utilized. The first PCB has two trace lines on the bottom side, while the top surface of the second PCB is a ground plane. The O-Clip under test is soldered on the bottom PCB. When the two PCBs are assembled to form the test fixture, they are aligned in such a way that one of the trace lines will properly contact the top contact point of the O-Clip. With proper control of the spacing between the two PCBs, the O-Clip is engaged connecting the trace and the ground plane in the middle of the transmission line formed by the trace and the ground plane. The other trace line, at the same time, forms another transmission line referencing the ground plane, which has the same geometry as the first one to be used for fixture removal. Taking an S parameter measurement of the two transmission lines with and without the O-Clip connection allows for the impedance of the O-Clip to be extracted using the proposed de-embedding method. The distance between the transmission lines is long enough that the coupling between them can be neglected. Using the proposed de-embedding method, the impedance of the O-Clip is found by removing the loss effect and phase shift of the imperfect transmission line, along with removing the effect of the discontinuity created by the connectors at the ends of the transmission line.

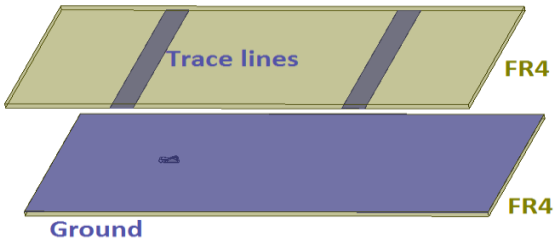

Figure 2.2. Measurement setup of the De-embedding method

2.1. DE-EMBEDDING METHOD

A De-embedding method will be applied to remove the fixture effects of the measurement setup, hence only the electrical performance of the DUT is obtained.

2.1.1. Basic Model. Practically, O-Clips are used as board to board connectors. A microstrip transmission line is formed from the copper trace line in the first PCB and the ground plane in the second PCB as shown in Figure 2.3, even though, in this case, the dielectric layer between them is air. To measurement the S-parameters, two vertical-mount coaxial connectors are added to the two ends of the transmission line. The outer conductor of the coaxial connector is connected to the ground plane, and the inner conductor is connected to the trace line. The O-Clip is placed in the middle of the transmission line as described before.

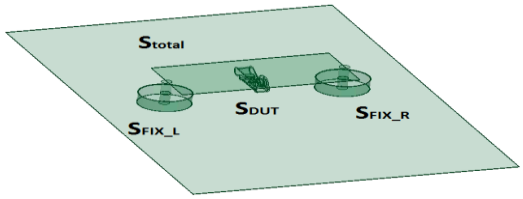

Figure 2.3. De-embedding model

$S_{total}, S_{FIX\_L}, S_{DUT}$, and S_{FIX_R} denote the S parameters for the total structure, the fixture on the left side of the DUT, the DUT (O-Clip), and the fixture on the right side of the DUT. To find S_{DUT} [3], $S_{total}, S_{FIX\_L}, S_{FIX\_R}$ must be known. In other words,

$$S_{total} = S_{FIX\_L} \otimes S_{DUT} \otimes S_{FIX\_R} \tag{2.1}$$

where $\otimes$ represents S-parameter cascading. In this equation, once three of these four S parameters are known, the last one can be derived.

2.1.2. Automatic Fixture Removal. If the O-Clip under test is placed in the middle of the transmission line, using symmetry, the S parameters of the right fixture and the S parameters of the left fixture are in mirror symmetric relationship, i.e.,

$$\begin{bmatrix} S_{11}^{FIX\_L} & S_{12}^{FIX\_L} \\ S_{21}^{FIX\_L} & S_{22}^{FIX\_L} \end{bmatrix} = \begin{bmatrix} S_{22}^{FIX\_R} & S_{21}^{FIX\_R} \\ S_{12}^{FIX\_R} & S_{11}^{FIX\_R} \end{bmatrix} \tag{2.2}$$

In order to obtain the S-parameters of the fixtures, the second transmission line is used as a "2X through".Cascading the left fixture with the right fixture gives us the 2X through:

$$S_{2X}^{THU} = S_{FIX\_L} \otimes S_{FIX\_R} \tag{2.3}$$

$$\begin{bmatrix} S_{11}^{TRU} & S_{12}^{TRU} \\ S_{21}^{TRU} & S_{22}^{TRU} \end{bmatrix} = \begin{bmatrix} S_{11} & S_{12} \\ S_{21} & S_{22} \end{bmatrix} \otimes \begin{bmatrix} S_{22} & S_{21} \\ S_{12} & S_{11} \end{bmatrix} \tag{2.4}$$

where $\begin{bmatrix} S_{11} & S_{12} \\ S_{21} & S_{22} \end{bmatrix}$ is the matrix representation of S_{FIX_L}.Since the fixtures are reciprocal, $S_{21} = S_{12}$. So only three unknowns S_{11}, S_{21} and S_{22} exist in S_{FIX_L}. Due to the symmetrical property of the 2X through, the following relationship for S_{2X}^{THU} also holds:

$$S_{11}^{TRU} = S_{22}^{TRU}, S_{12}^{TRU} = S_{21}^{TRU} \tag{2.5}$$

Currently, there are three unknowns with only two equations. To gain a third equation, a TDR is performed on the S_{2X}^{THU} and the corresponding TDR of the left fixture is further obtained [4]. By solving the three equations, S_{FIX_L} and S_{FIX_R} are obtained. Then, through (1), S_{DUT} for the O-Clip can be solved. Converting from the S parameters to Z parameters, the impedance of the O-Clip which is equal to Z_{21} can be derived as [5]

$$Z_{21} = \frac{2S_{21}}{\triangle S} Z_0 \tag{2.6}$$

where $\triangle s = (1-S_{11})(1-S_{22}) - S_{12}S_{21}$, and Z_0 is the characteristic impedance of the transmission line.

2.1.3. S Parameters and Impedance Results. The 3D models shown in Figure 2.4 are simulated in HFSS, a finite element method based tool from Ansys.

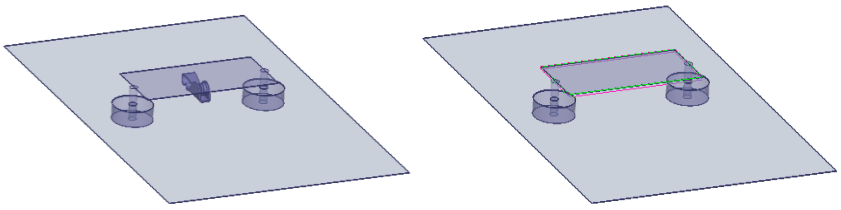

(a) (b)

Figure 2.4. HFSS model (a) De-Embedding structure (b) 2X through

Firstly, with the S_{2X}^{THU} from the HFSS 2X through structure, S_{FIX_L} and S_{FIX_R} are obtained. The results for S_{FIX_L} are shown in Figure 2.5. The S_{2X}^{THU} result is further compared with the cascaded S parameters of the left and right fixtures in Figure 2.6, to demonstrate that the fixture characterization is correct.

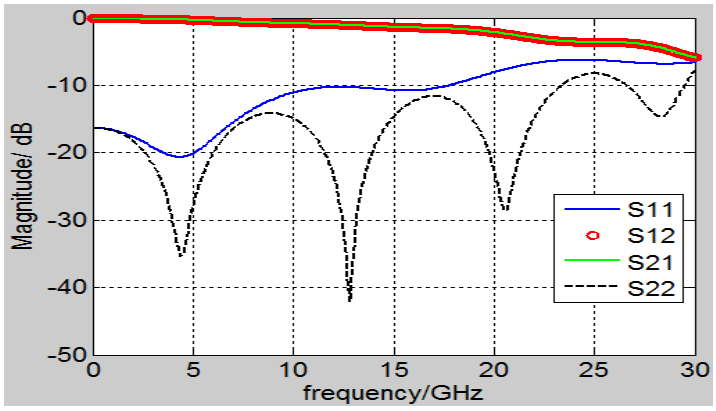

Figure 2.5. S parameters of the left fixture

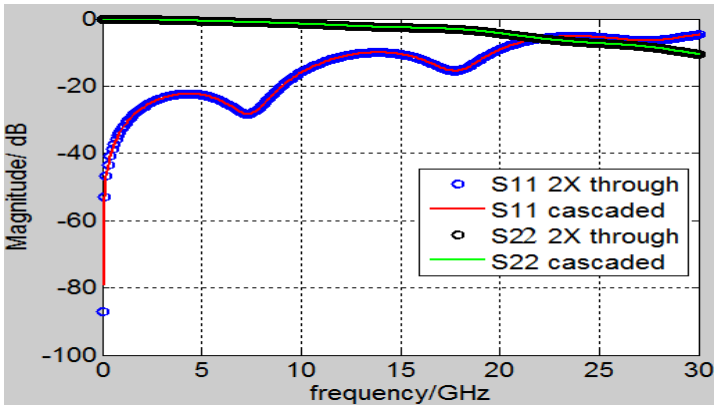

Figure 2.6. S parameters of right-left fixture cascaded and 2X through

When the S parameters of the two fixtures are known, together with the overall S parameters from the HFSS simulation, the S parameter for the O-Clip can be solved. A comparison between the magnitude of the overall S_{21} and the S_{21} of the O-Clip with the fixtures de-embedded is shown in Figure 2.7.

Converting the S parameters to Z parameters, the real part and imaginary part of the O-Clip impedance are obtained and shown in Figure 2.8. At low frequencies, the O-Clip behaves inductively; however, when the frequency goes up to 25.9 GHz, a resonance occurs and the O-Clip behaves capacitively right after the resonance.

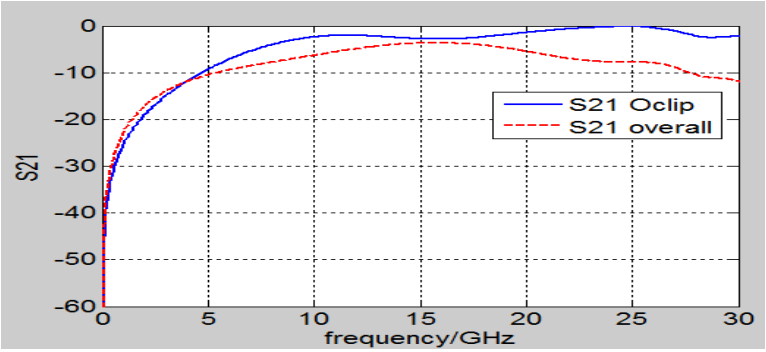

Figure 2.7. Comparison between S_{21} of O-Clip and S_{21} Overall

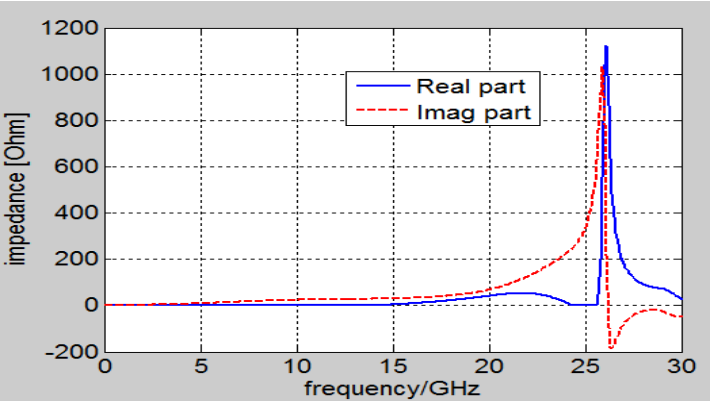

Figure 2.8. Real part and imaginary part of the O-Clip

2.2. ELECTROMAGNETIC MODELING FOR VALIDATION

In the de-embedding model, the O-Clip is placed in the middle of a transmission line for two reasons. One reason is that the ports are well defined making measurements easier to implement. The other reason is that it's closer to the real application of the O-Clip. The O-Clip is mostly used as a board- to-board connection where current flows from the peak point of the O-Clip, through the O-Clip, and to the ground plane.

In order to understand the resonance of the impedance in the frequency range of 0-30 GHz, more details of the O-Clip need to be examined. Inspired by the idea that two current flow paths exist in the O-Clip, it is cut into two pieces in Figure 2.9. The

impedances of these two parallel pieces can be used to explain the electrical performance of the O-Clip over frequency.

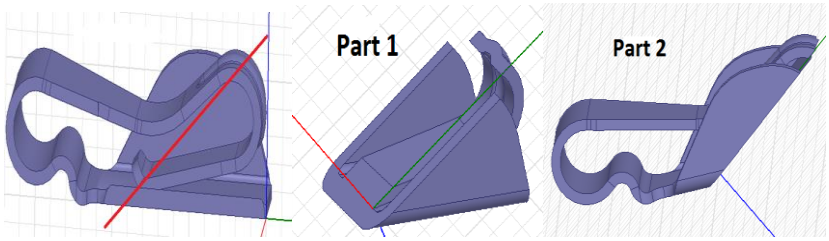

(a) (b) (c)

Figure 2.9. Model of: (a) whole O Clip; (b) One half: part 1; (c) One half: part 2

Using the driven modal solution type in HFSS, a lumped port was added in the cutting plane to get the impedance of the structure. Then the two blocks were treated as parallel blocks to get the overall impedance of the structure.

2.2.1. Impedance of Part 2. For part 1, the real part and imaginary part of the impedance are shown in Figure 2.10. In this frequency range, the imaginary part is dominated by inductance since it's proportional to frequency. The real part increases with frequency due to the skin effect.

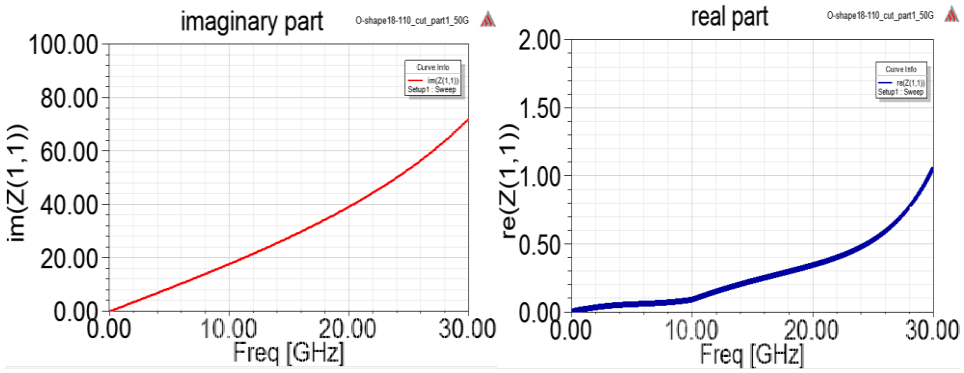

Figure 2.10. Part 1: imaginary part and real part of the impedance

2.2.2. Impedance of Part 2. For part 2, the real part and imaginary part of the impedance are shown in Figure 2.11.

In this frequency range, the impedance changes from inductive to capacitive because in this frequency range ,part 2 can no longer be regarded as an electrically small lumped element. In fact, part 2 is more like a shorted transmission line. The input impedance of a short circuited TX line is given as

$$Z_{in} = Z_0 \frac{Z_L + Z_0 \tanh(\gamma L)}{Z_0 + Z_L \tanh(\gamma L)} \xrightarrow{Z_L=0} Z_0 \tanh(\gamma L) \tag{2.7}$$
$$\gamma = \alpha + j\beta$$

where Z_0 is the characteristic impedance of the equivalent transmission line, γ is the complex propagation constant, α is the attenuation constant, and β is the phase constant. So when the frequency goes higher, the impedance will alternate between inductive and capacitive.

Using the same theory, part 1 can also be treated as a short circuited TX line. Since the dimension of part 1 is much smaller than that of part 2, the impedance is inductive in the frequency up to 30 GHz.

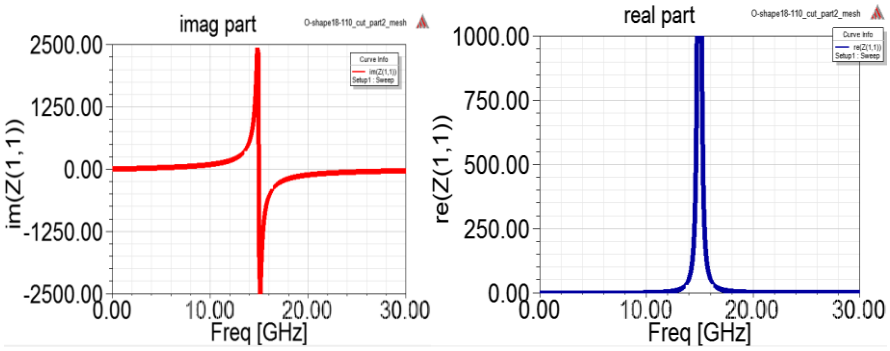

Figure 2.11. Part 2: imaginary part and real part of the impedance

2.2.3. Validation Using HFSS Simulation. The two parts are treated as parallel electric blocks to get the overall impedance of the structure. Results are then compared with the results from the de-embedding method. The real part and imaginary part comparisons are shown in Figure 2.12. The results agree roughly well in most of the frequency range. At high frequencies, the current distribution in the two pieces is different from the original O-Clip placed in the middle of a two boards, which may describe there is some mismatch in the impedance. Last but not the least; the O-Clip is regarded as a point in the de-embedding method. Error will be introduced at high frequencies since the dimension effect of the O-Clip may start to appear.

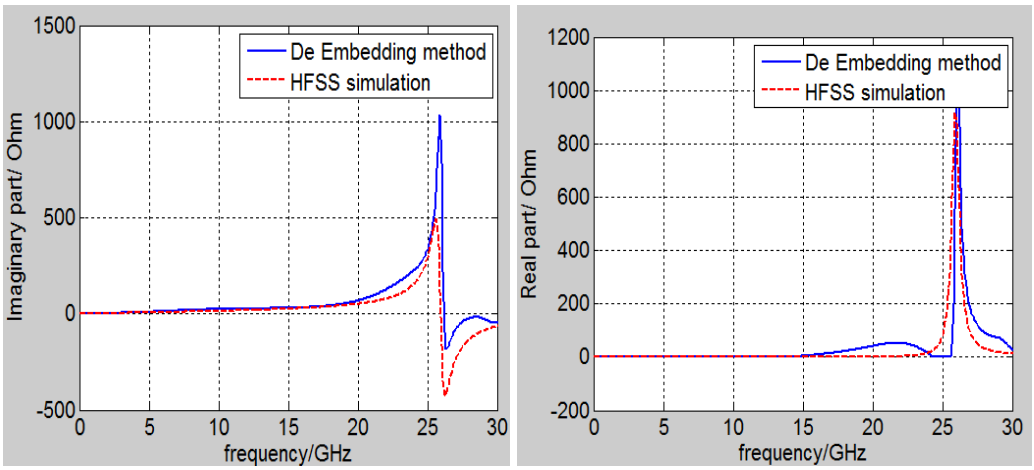

Figure 2.12. Imaginary part and real part comparisons

2.3. MEASUREMENT VALIDATION

Test boards are built to measure the O shape spring contacts and also the O shape spring contacts. Typical shape of the O and C shape spring contacts are shown in Figure 2.13.

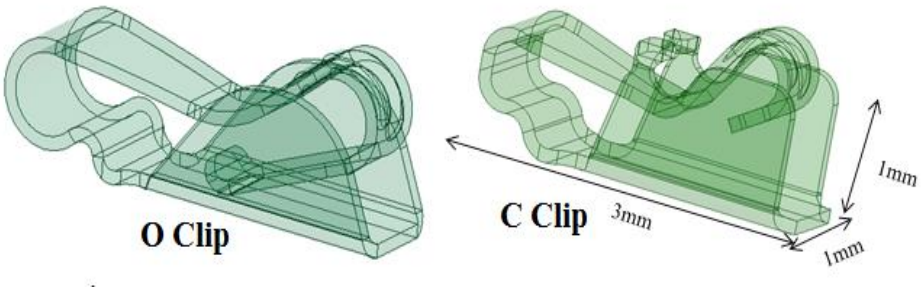

Figure 2.13. Typical shape of O and C clips

2.3.1. Measurement Results of O and C Clips up to 10GHz. A test vehicle is built to fulfill the following requirements:

- Spring contact needs to be activated, the clip impedance is measured when it is compressed at working height
- High repeatability
- For the test vehicle, fixture effect needs to be eliminated to obtain the accurate impedance (typically a small value)

The 1 to 1 comparison between the simulation model and real PCB is shown in Figure 2.14. Two PCBs of equal size are utilized. The first PCB has two trace lines on the top side, while the bottom surface of the second PCB is a ground plane. The O-Clip under test is soldered on the trace. When the two PCBs are assembled to form the test fixture, they are aligned in such a way that one of the trace lines will properly contact the top contact point of the O-Clip. With proper control of the spacing between the two PCBs, the O-Clip is engaged connecting the trace and the ground plane in the middle of the transmission line formed by the trace and the ground plane. The other trace line, at the same time, forms another transmission line referencing the ground plane, which has the same geometry as the first one to be used for fixture removal. Taking an S parameter

measurement of the two channels with and without the O-Clip connection allows for the impedance of the O-Clip to be extracted using the proposed de-embedding method.

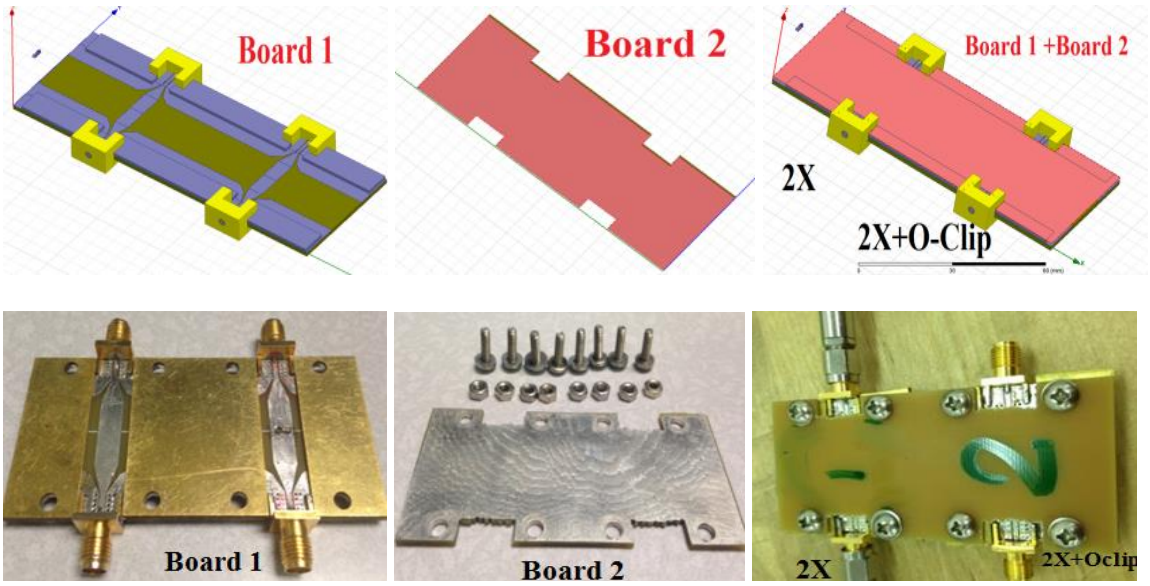

Figure 2.14. HFSS model and its corresponding real PCB

More details of the two channels with and without the O clip are shown in Figure 2.15. Board 2 will be placed on top of the spacer when the measurements are actually taken.

The S parameters for the 2X channel and the 2X+DUT channel are then measured using VNA. De-embedding method will be applied to remove the fixture effect, and then S parameter of the DUT will be obtained. The whole procedures are shown in Figure 2.16.The original height of the DUT O clip is 2.8mm. It's compressed to 2.3mm at its working height, since the height of the copper spacer is 2.3mm.When the whole test board is assembled, the O clip in the middle is compressed to the height of the copper spacer.

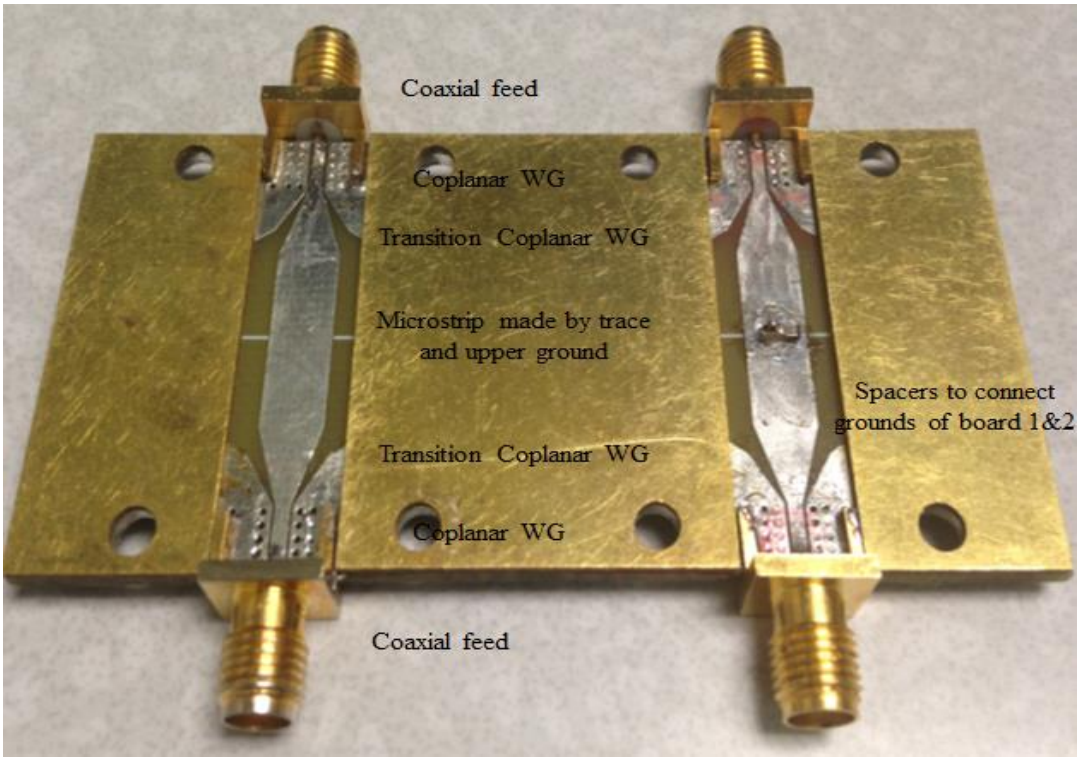

Figure 2.15. Details of the measurement board

3D model is also built in HFSS, which has the same geometry with the measurement. The same de-embedding procedures will be applied to the simulated S parameters, so similarly the impedance of the DUT can be obtained. The imaginary part of the impedance due to the inductance is shown in Figure 2.17.

The result comparison between measurement and simulation shows good agreement with a difference less than 4dB in the frequency range from 10 MHz to 10 GHz. A clear 20 dB/decade increase indicates the inductance behavior.

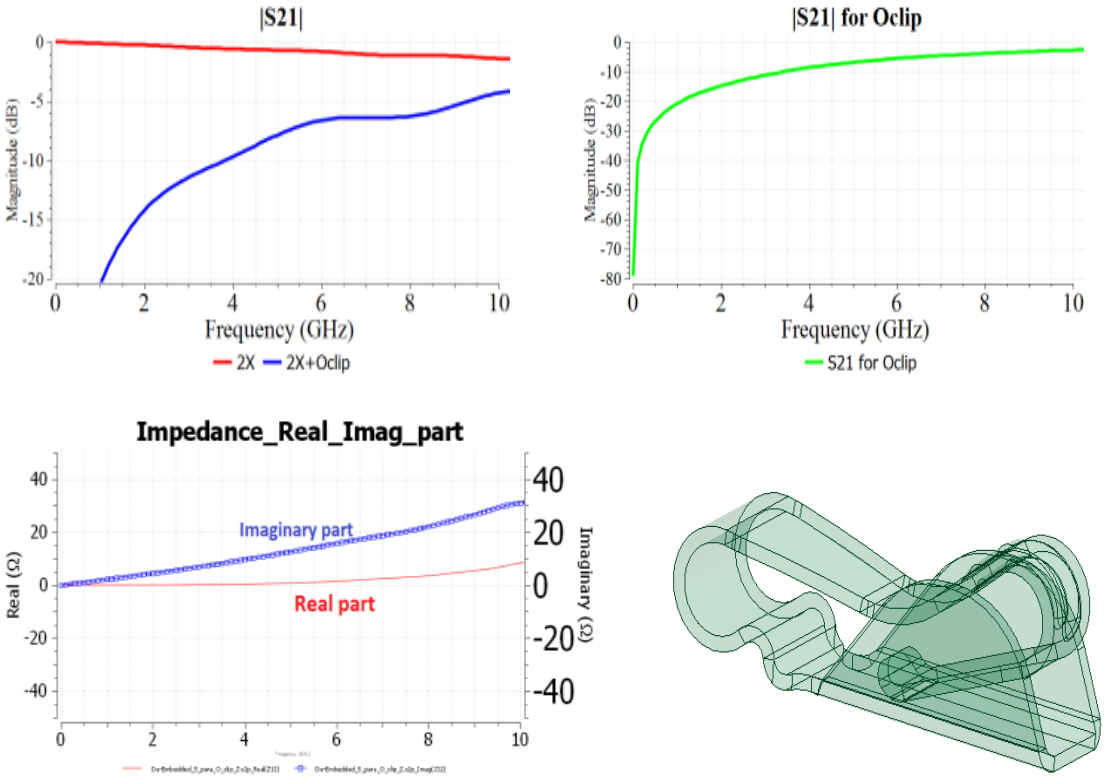

Figure 2.16. Procedures of applying de-embedding method

The same set of measurements can be performed on the C clip,which is also compressed to work at 2.3mm.Results compariosn of the O and C clip are shown in Figure 2.18. The O clip has a smaller inductance than the C clip. Also the impedance trend shows that the C clip is reaching its self-resonant frequency at around 10 GHz. However, the resonant frequency of the O clip may be well beyond 10 GHz. The reason is the C clip can also be roughly regarded as a short-circuit TX line, whose length is much longer than that of O clip. It will not only provide a bigger inductance, but also a smaller resonant frequency compared to the O clip.

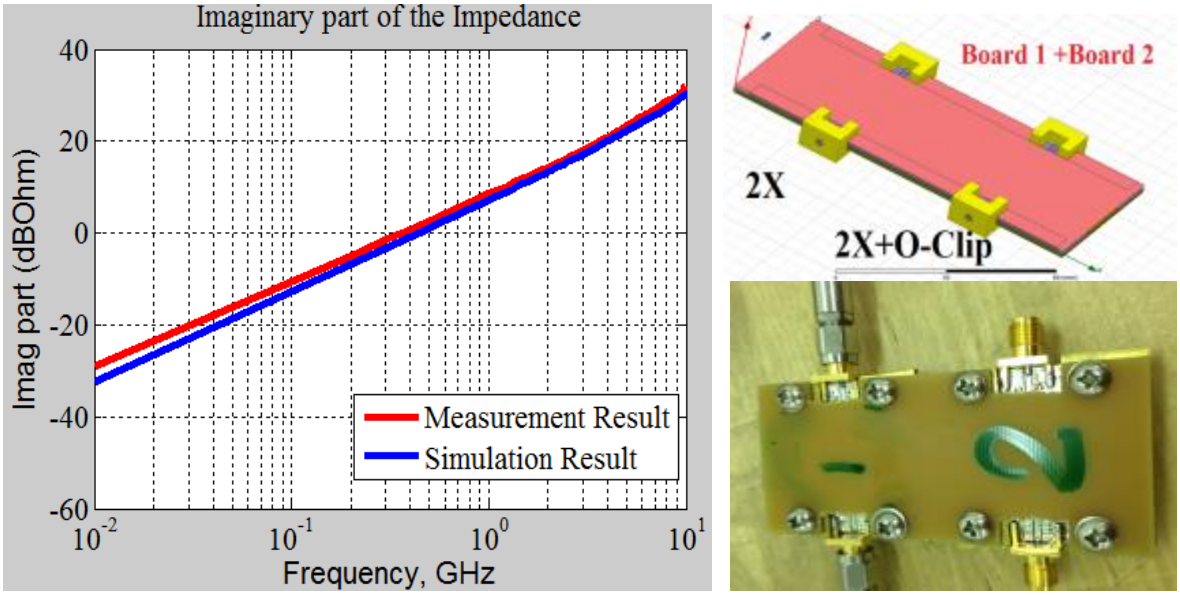

Figure 2.17. Imaginary part of the impedance from measurement and simulation data

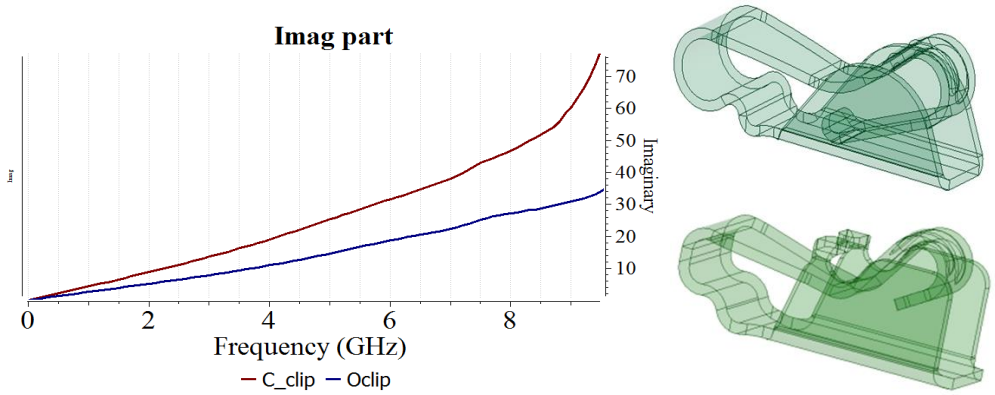

Figure 2.18. Imaginary part comparison between O and C clip

Similar test vehicles are built to measure O clip at different working height. Because different O clip or even one specific O clip will have different working height, different copper spacers need to be used. Each copper spacer will correspond to a test vehicle, which compress the DUT to the height of the spacer. A typical case of real world

application is like this: the same O clip is used, but works at different height. Figure 2.19 shows the impedance result of that; a 2.2mm O clip is compressed and measured at 2.3mm, 2.6mm. The 2.2mm O clip which works at 2.60mm has a bigger inductance than the 2.2mm O clip which works at 2.3mm, since the 2.6mm O clip will introduce a bigger loop area when used as the board to board connection.

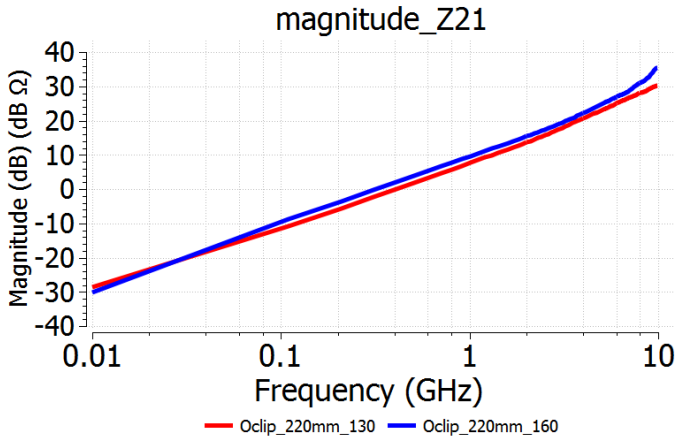

Figure 2.19. Magnitude of the impedance of O clip at different working heights

Another typical case of real world application is like this: Different O clip is used to compressed and work at the same height. Figure 2.20 shows the geometry of 3 different O clips, 2.5 mm, 2.8 mm, 2.2 mm. All of them are measured using the same test vehicle. This test vehicle compresses all the clips to the same working height, 2.3mm.

The imaginary part of the impedance is compared for the above 3 cases, the results are shown in Figure 2.21. For frequency up to 10 GHz, the O-clip is still in the inductive region. And the inductance is mainly determined by the short path of the O clip. For the per unit length inductance, wider trace will have smaller PUL inductance, because current can flow more freely on the surface. According to Figure 2.20, 2.2 mm O

clip has the widest path for current flowing, so it will have least inductance, thus least impedance.

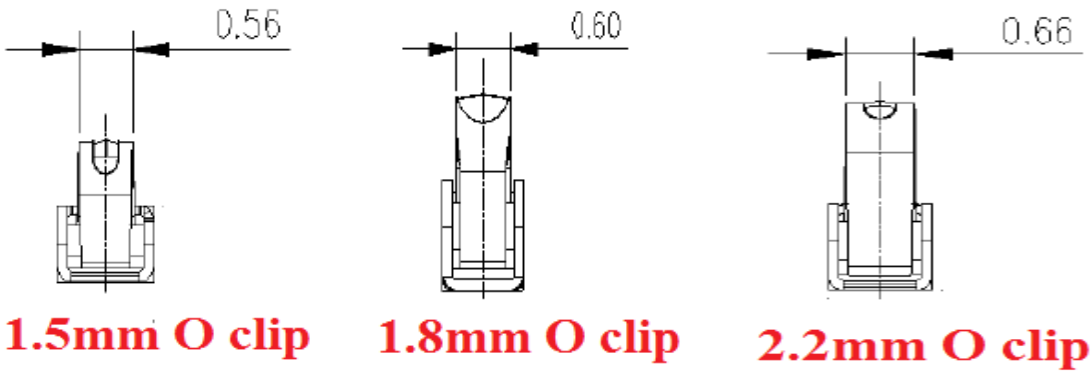

Figure 2.20. Geometry of 3 different O clips

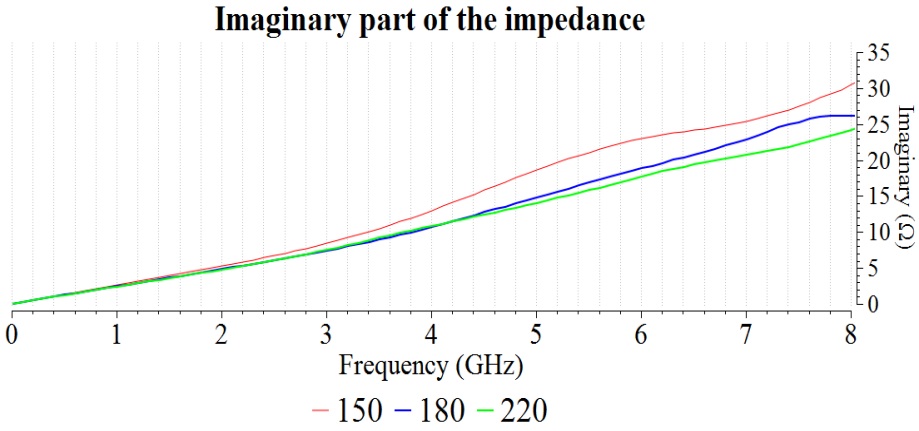

Figure 2.21. Imaginary part of the impedance of different O clip at same heights

2.3.2. Measurement Results of O and C Clips up to 20 GHz. Previous simulation and measurement results show that O clip have two advantages over C clip: smaller self-inductance value, bigger self-resonant frequency. These two advantages can't be observed using a 10 GHz test vehicle. While building a 20 GHz test vehicle is necessary, it's hard to design. In previous 10 GHz test vehicle design, a 33$ board from

4PCB is used, which use FR4 as substrate. The new design is layout at AP circuit, which uses more expensive Rogers 4350b as the substrate.

In order to make De-Embedding method work good, a 2X through channel should fulfill the following conditions:

- Insertion loss |S21| curve is relatively smooth
- Reflection loss |S11| is well below |S21|.

The test vehicle is simulated in HFSS, as shown in Figure 2.22. The S parameters of the 2X through channel are shown in Figure 2.23.

Clearly, the simulated S parameters in the figure below fulfill the two requirements above.

The real PCB is shown in Figure 2.24; it also shows how the whole test vehicle is assembled. Four conductive foams are added in the middle to act as the spacers, since irregular shape of copper spacer is difficult to manufacture. Two channels will be measured: one is 2X through; another one is 2X thru + DUT.

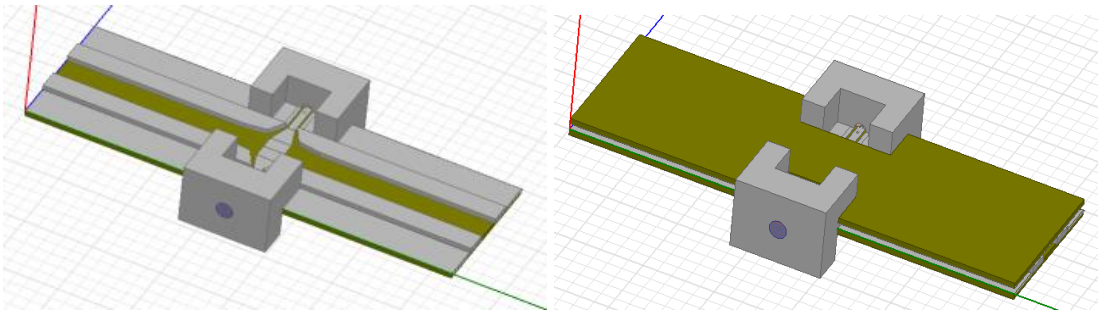

Figure 2.22. HFSS model of the 2X through channel

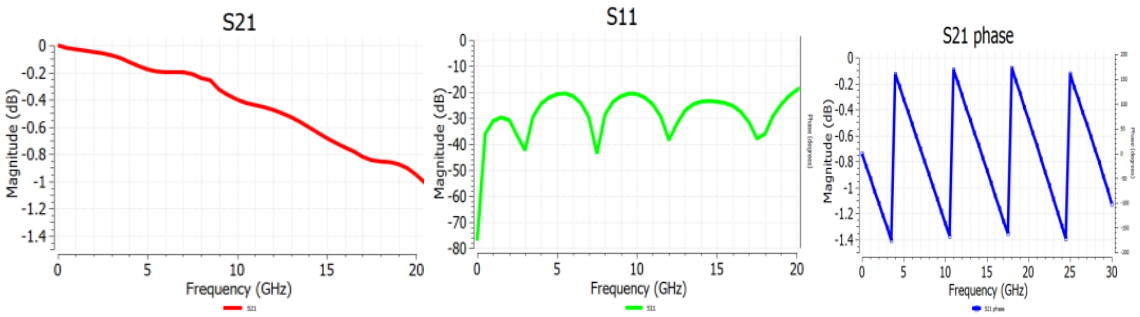

Figure 2.23. Simulated S parameters of 2X through channel by HFSS

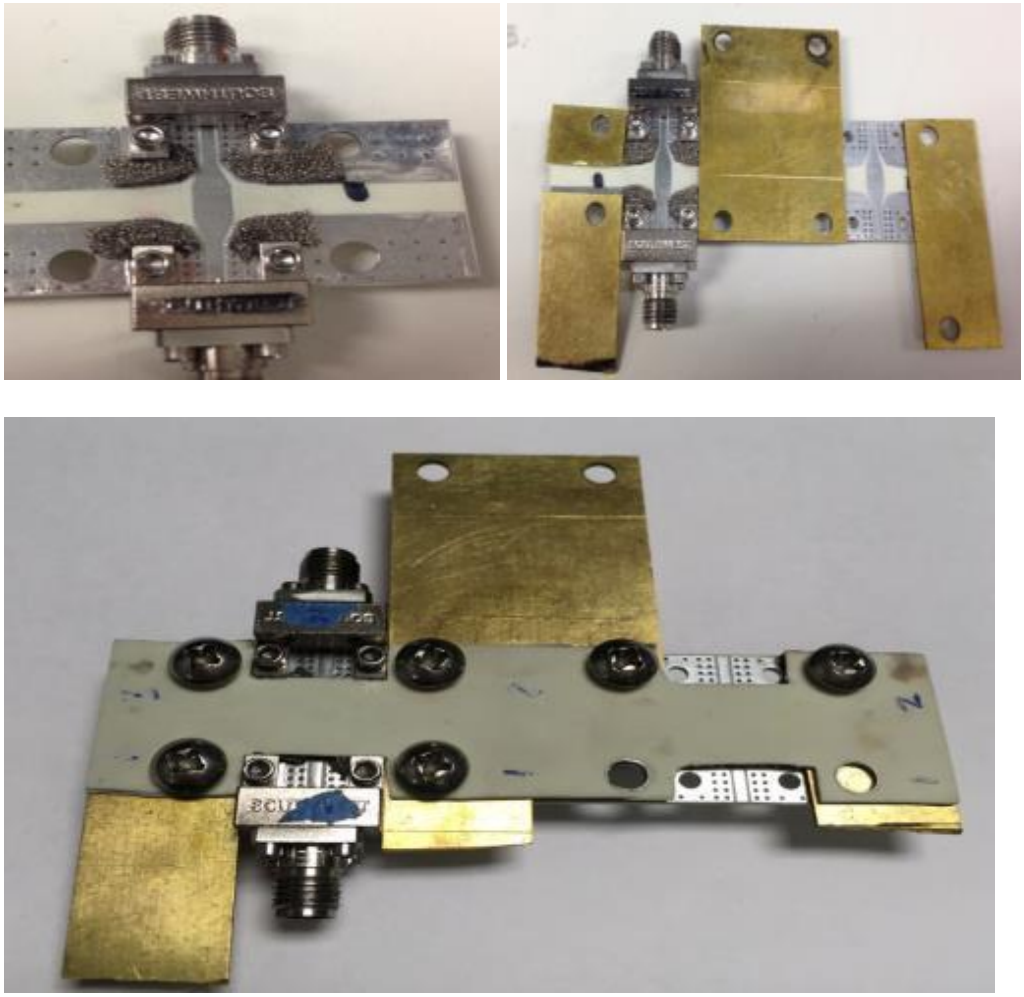

Figure 2.24. Parts and assembling processing of the 20 GHz test vehicle

The measured S parameters of the 2X through channel are shown in Figure 2.25. For the measured S parameters, the insertion loss |S21| curve is relatively smooth; reflection loss |S11| is well below |S21|.

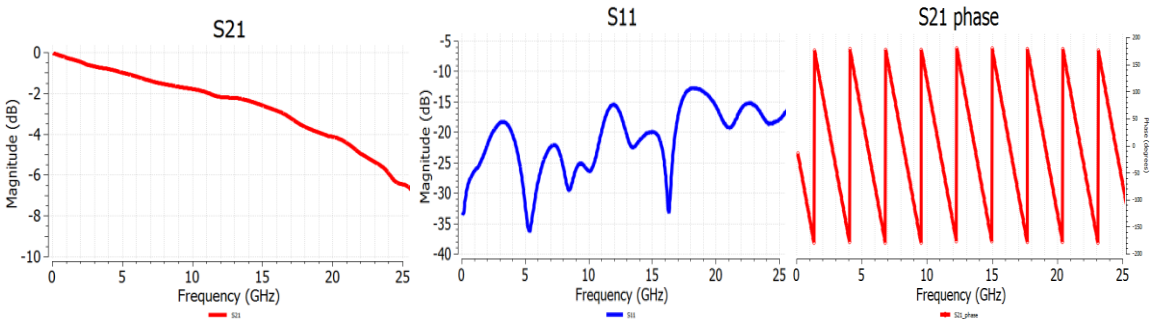

Figure 2.25. Measured S parameters of the 2X through channel

In this study, to reduce the errors, the same 2X through channel will be used in the 2X+DUT channel. Details about how the clip is assembled in the test vehicle are shown in Figure 2.26. VNA is used to measure the 2X+DUT channel, the S parameter results of the 2X+DUT channel are shown in in Figure 2.27.

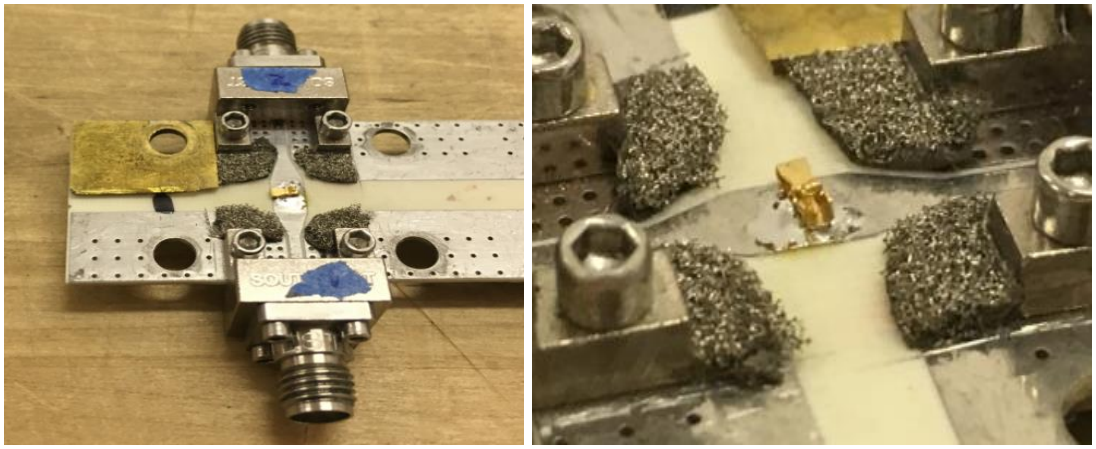

Figure 2.26. Assembling processing of the C clip in the test vehicle

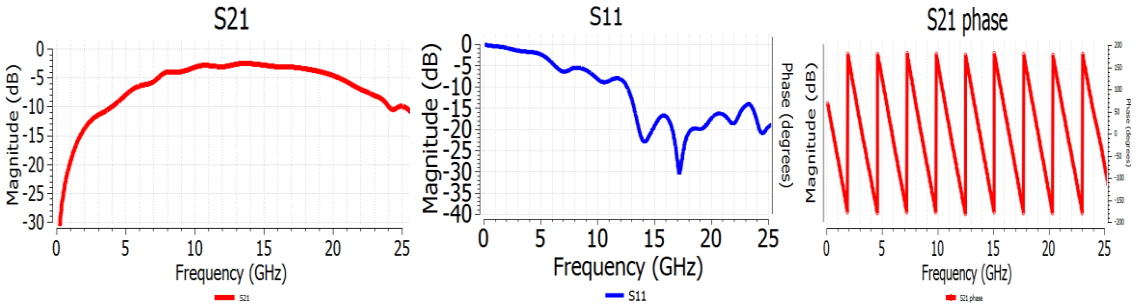

Figure 2.27. Measured S parameters of the 2X+DUT channel

Smart Fixture De-Embedding method is used to derive the S parameter of the 1X from the 2X through channel. The S parameter and TDR comparisons between 1X and 2X channel are shown in Figure 2.28.

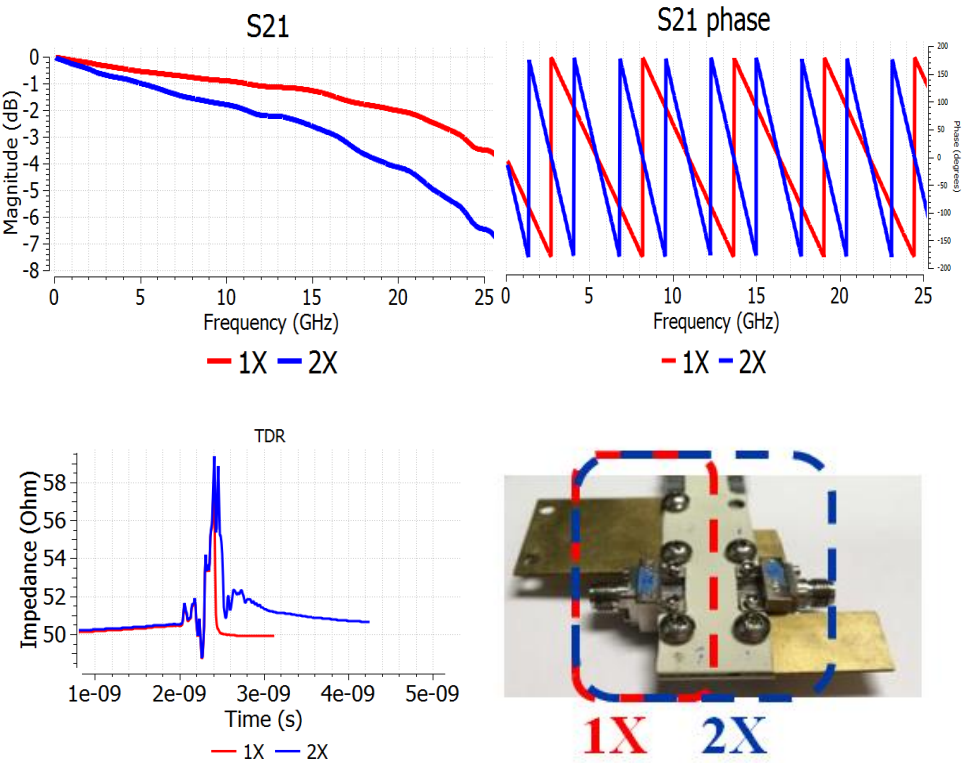

Figure 2.28. S parameter and TDR comparisons of 1X and 2X channel

Applying Smart Fixture De-Embedding method, S parameters of the DUT can be further obtained, which are shown in Figure 2.29.

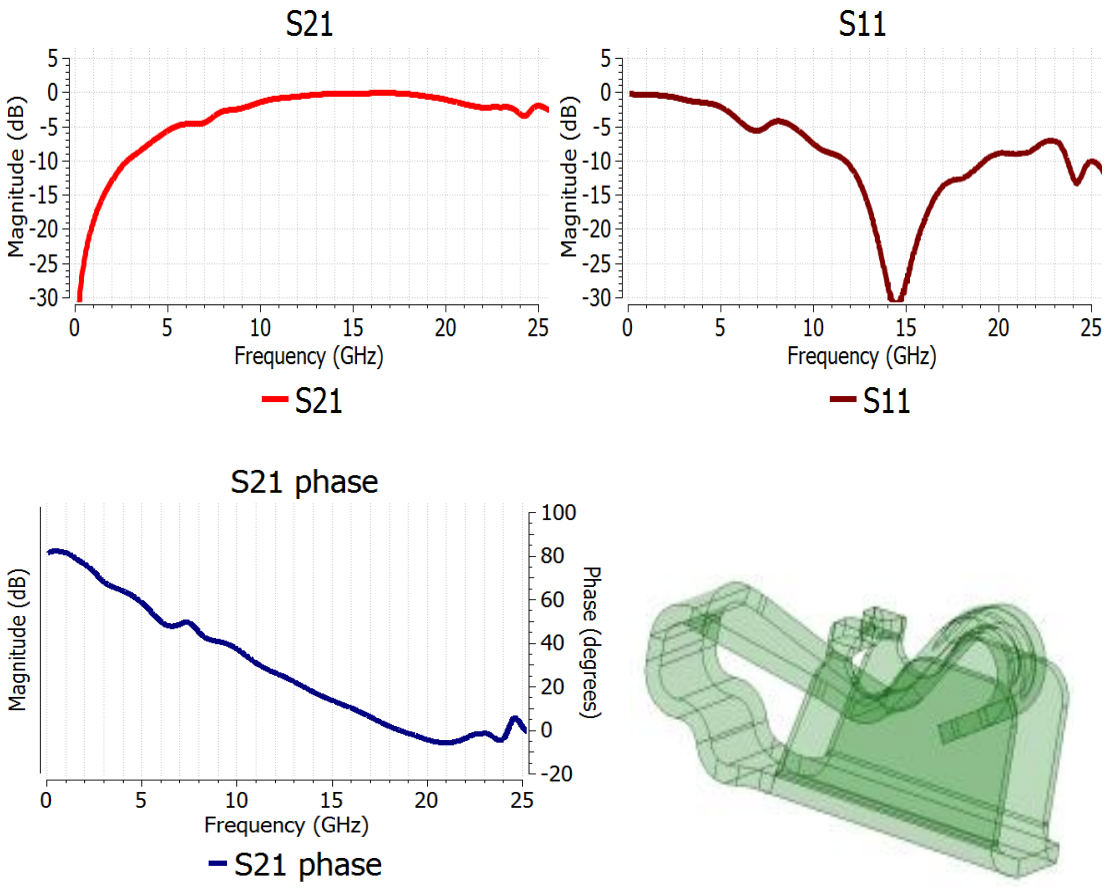

Figure 2.29. S parameter of the DUT C clip

Converting the S parameters to Z parameters, the magnitude and phase of the O-Clip impedance are obtained and shown in Figure 2.30. For C clip, self-resonant frequency is measured to be 16.5 GHz. When the magnitude of Z21 reaches its max value, the phase of Z21 quickly changes from 90˚ to -90˚, and the DUT turns from inductive behavior to capacitive behavior.

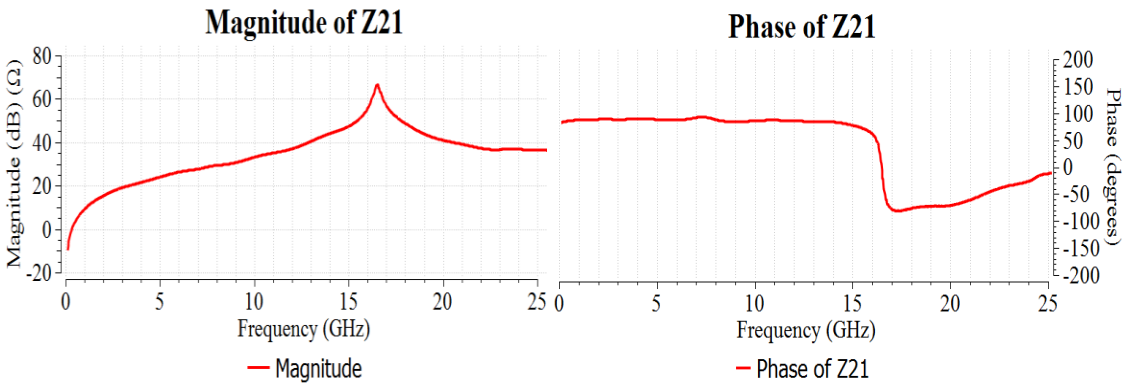

Figure 2.30. Magnitude and phase of C clip impedance

The same measurement procedures are applied to measure the impedance of the O clip. Both of the clips has 2.3mm as the original height, are compressed to work at 0.8mm since the height of the spacer is 0.8mm. Impedance comparisons of the C and O clip with same profile are shown in Figure 2.31. In addition to lower impedance due to a lower inductance, the O clip has a self-resonant frequency higher than 25 GHz, which is higher than the C clip. Below 25 GHz, O clip clearly shows inductive behavior, and the magnitude of its impedance increases by 20 dB/decade.

The reasons for adding conductive foam at the 2X through channel, as shown in Figure 2.32, is because by doing this, higher order modes of EM wave can be suppressed. |S21| comparisons of the 2X through channel with and without the conductive foam are shown in Figure 2.33. Using conductive foam clearly gives a better |S21| slope, which is required for a good de-embedding result.

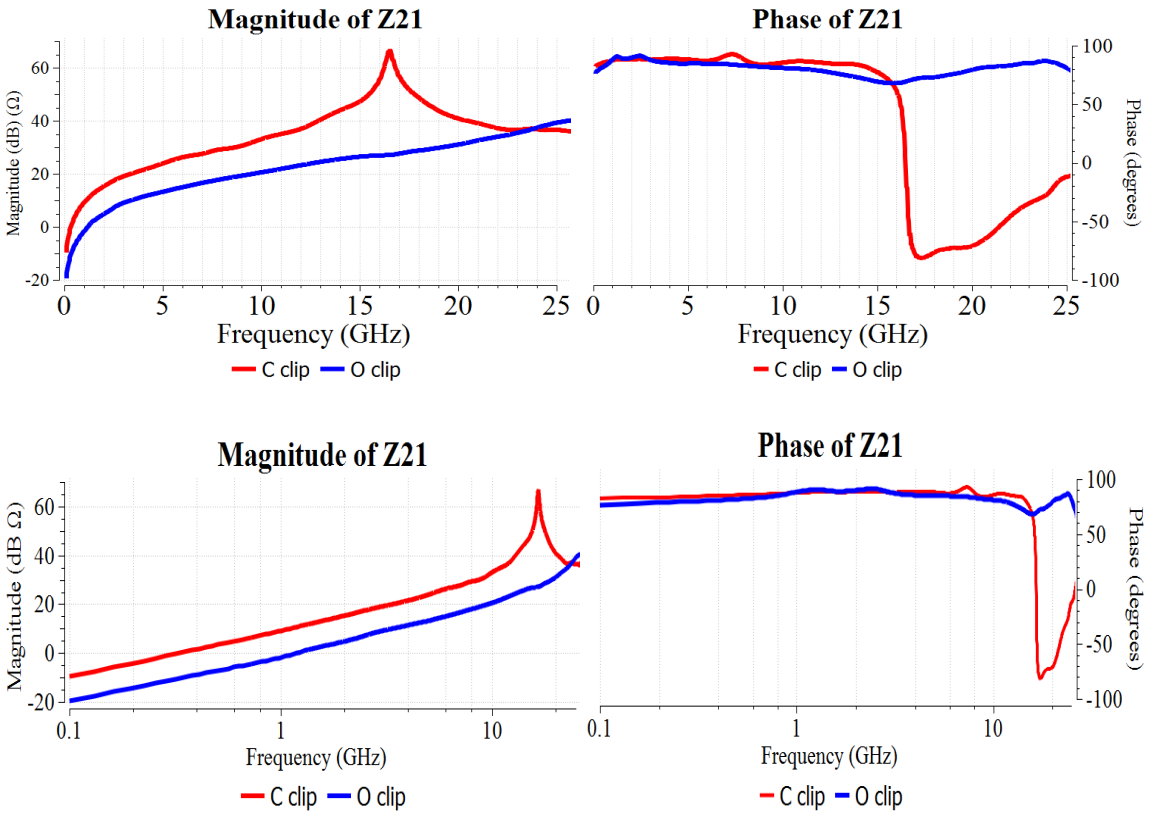

Figure 2.31. Magnitude and phase of C and O clip impedance

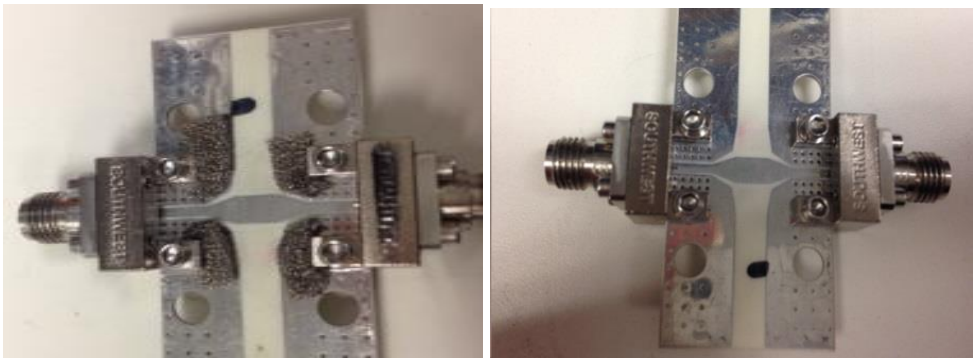

Figure 2.32. PCB with and without the conductive foam

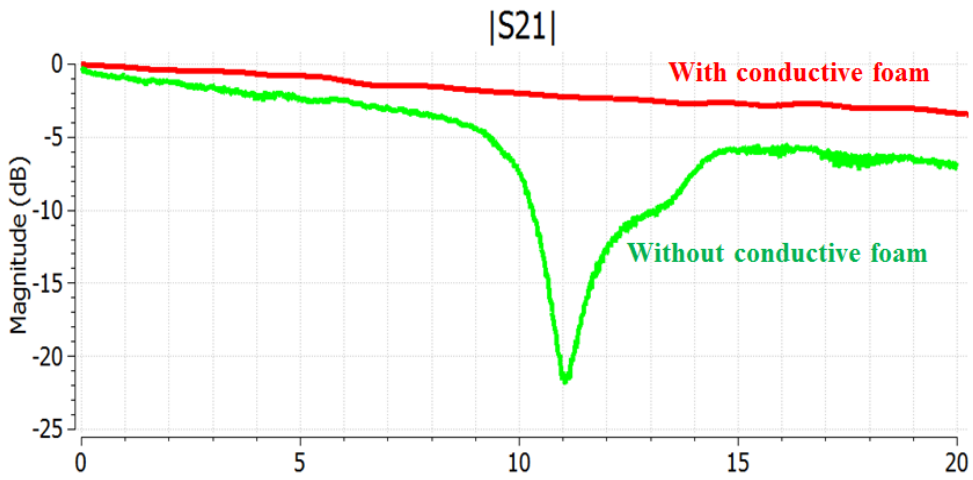

Figure 2.33. |S21| comparison with and without the conductive foam

One difference between a TEM mode and high order mode EM wave is that only tangential wave exists for TEM wave, normal component is zero; while normal component exists for high order mode EM wave. The 2X channels with and without the conductive material are modeled and simulated in HFSS.

At the cross-section of the transition CPW part, normal H field is plotted and compared in Figure 2.34. Both plots use the same scale, clearly higher order TE mode is observed when no conductive material is used. With conductive material, EM is still quasi-TEM.

Similar comparison can be shown in Figure 2.35; normal H field over tangential H field ratio is compared for with and without conductive material cases. Without conductive material, a significant amount of higher mode TE mode can be seen, while the EM can still be treated as quasi-TEM mode if conductive material is added.

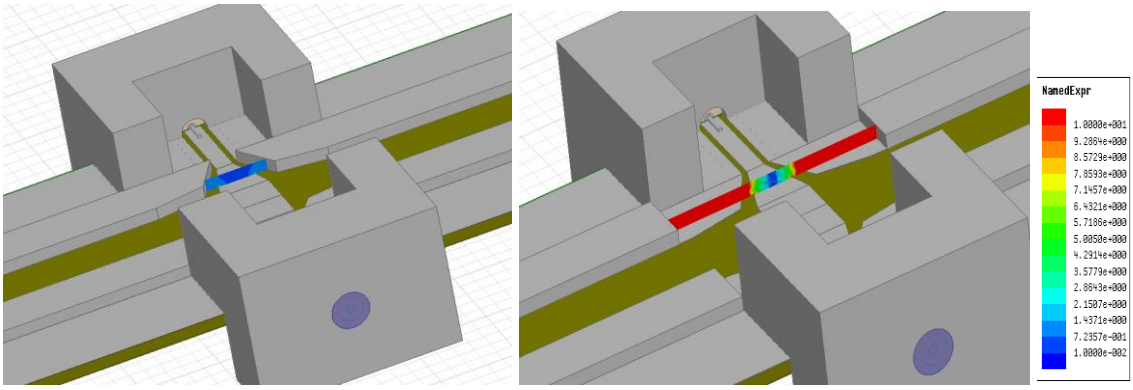

(a) (b)

Figure 2.34. Normal H field at the cross section, with (a) and without (b) conductive material

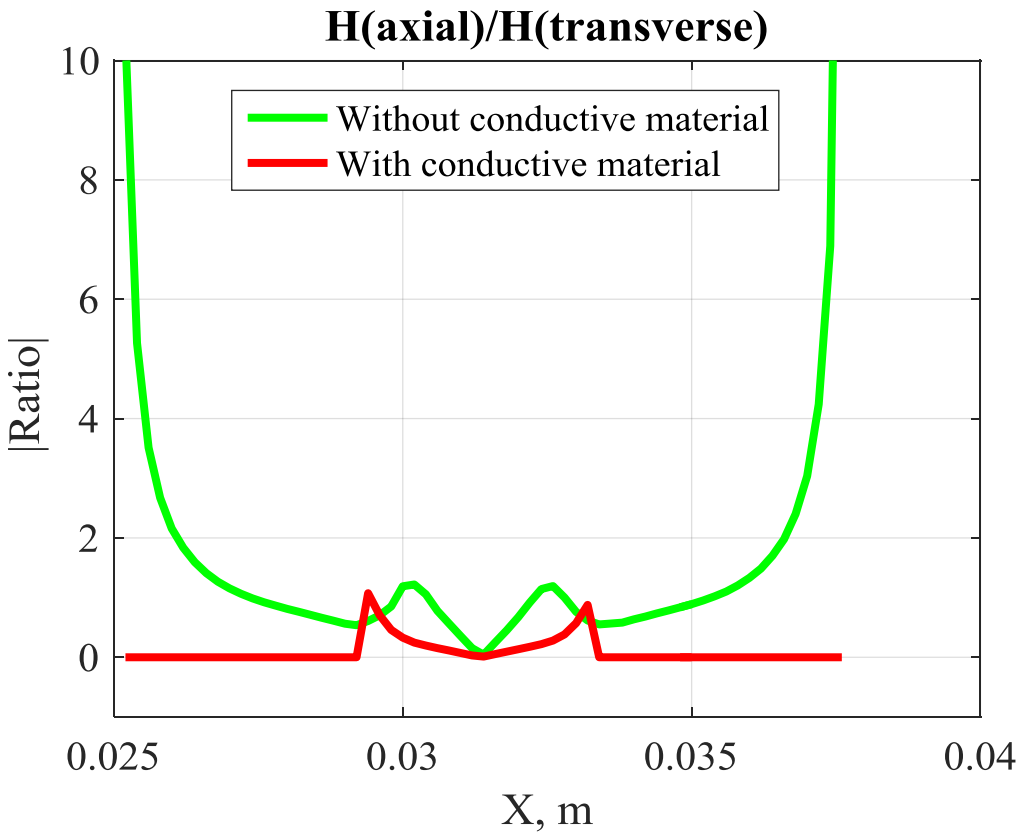

Figure 2.35. Ratio between normal H field over tangential H field, with and without conductive material

3. RADIO-FREQUENCY INTERFERENCE ESTIMATION USING EQUIVALENT DIPOLE-MOMENT MODELS

3.1. EQUIVALENT DIPOLE-MOMENT MODELS

From the multipole expansion of an electromagnetic radiation source [6] [10], an arbitrary electrically small source can be approximately replaced by six dipoles: three electric dipoles denoted Px , Py , and Pz , and three magnetic dipoles denoted Mx ,My , and Mz . These dipoles together generate approximately the same fields as the source. For a lot of applications, the noise source is usually located closely on a large ground plane. In those situations, the radiation from tangential electric dipoles Px,Py and vertical magnetic dipoles Mz will almost be cancelled by their images[11]. Thus, in Cartesian coordinates, just the vertical electric dipoles (Pz) and tangential magnetic dipoles (Mx,My)are enough for modeling.

The tangential E and H field radiated by P_z, M_x and M_y dipoles can be samely written as in [12] [13].

$$E_x = -j\frac{k_0\eta_0}{4\pi}\left\{\left[\frac{(z-h)(x-x')}{r_1^2}q_1(r_1)+\frac{(z+h)(x-x')}{r_2^2}q_1(r_2)\right]P_z + \left[\frac{(z-h)}{r_1}q_3(r_1)+\frac{(z+h)}{r_2}q_3(r_2)\right]k_0M_y\right\} \tag{3.1}$$

$$E_y = -j\frac{k_0\eta_0}{4\pi}\left\{\left[\frac{(z-h)(y-y')}{r_1^2}q_1(r_1)+\frac{(z+h)(y-y')}{r_2^2}q_1(r_2)\right]P_z + \left[-\frac{(z-h)}{r_1}q_3(r_1)-\frac{(z+h)}{r_2}q_3(r_2)\right]k_0M_x\right\} \tag{3.2}$$

$$H_x = \frac{k_0}{4\pi}\left\{-\left[\frac{(y-y')}{r_1}q_3(r_1)+\frac{(y-y')}{r_2}q_3(r_2)\right]P_z \right. \\ +\left[-\frac{(y-y')^2+(z-h)^2}{r_1^2}q_1(r_1)+q_2(r_1)-\frac{(y-y')^2+(z+h)^2}{r_2^2}q_1(r_2)+q_2(r_2)\right]k_0 M_x \\ \left.+\left[\frac{(x-x')(y-y')}{r_1^2}q_1(r_1)+\frac{(x-x')(y-y')}{r_2^2}q_1(r_2)\right]k_0 M_y\right\} \tag{3.3}$$

$$H_y = \frac{k_0}{4\pi}\left\{\left[\frac{(x-x')}{r_1}q_3(r_1)+\frac{(x-x')}{r_2}q_3(r_2)\right]P_z \right. \\ +\left[-\frac{(x-x')^2+(z-h)^2}{r_1^2}q_1(r_1)+q_2(r_1)-\frac{(x-x')^2+(z+h)^2}{r_2^2}q_1(r_2)+q_2(r_2)\right]k_0 M_y \\ \left.+\left[\frac{(x-x')(y-y')}{r_1^2}q_1(r_1)+\frac{(x-x')(y-y')}{r_2^2}q_1(r_2)\right]k_0 M_x\right\} \tag{3.4}$$

Where k_0 is the free space wave number, η_0 is the wave impedance in vacuum; P_z is a complex number denoting the electrical dipole along z direction with unit of $A\cdot m$; M_x and M_y denote the magnetic current along x and y direction respectively with unit of $A\cdot m^2$.

$$r_1 = \left[(x-x')^2+(y-y')^2+(z-h)^2\right]^{1/2} \tag{3.5}$$

$$r_2 = \left[(x-x')^2+(y-y')^2+(z+h)^2\right]^{1/2} \tag{3.6}$$

$$q_1(r) = \left[\frac{3}{(k_0 r)^2}+j\frac{3}{k_0 r}-1\right]g(r) \tag{3.7}$$

$$q_2(r) = \left[\frac{2}{(k_0 r)^2}+j\frac{2}{k_0 r}\right]g(r) \tag{3.8}$$

$$q_3(r) = \left[\frac{1}{k_0 r}+j\right]g(r) \tag{3.9}$$

$$g(r) = \frac{e^{-jk_0 r}}{r} \tag{3.10}$$

Equation (3.1) through (3.4) can be simplified to the following matrix form as

$$\begin{bmatrix} E_x \\ E_y \\ H_x \\ H_y \end{bmatrix} = \begin{bmatrix} T_{E_x\_P_z} & 0 & T_{E_x\_M_y} \\ T_{E_y\_P_z} & T_{E_y\_M_x} & 0 \\ T_{H_x\_P_z} & T_{H_x\_M_x} & T_{H_x\_M_y} \\ T_{H_y\_P_z} & T_{H_y\_M_x} & T_{H_y\_M_y} \end{bmatrix} \begin{bmatrix} P_z \\ M_x \\ M_y \end{bmatrix} \tag{3.11}$$

Where $T_{E_x\_P_z}$, $T_{E_x\_M_y}$; $T_{E_y\_P_z}$, $T_{E_y\_M_x}$; $T_{H_x\_P_z}$, $T_{H_x\_M_x}$, $T_{H_x\_M_y}$; $T_{H_y\_P_z}$, $T_{H_y\_M_x}$ and $T_{H_y\_M_y}$ denote the transfer coefficient of field components that are caused by different dipole types. For example, the transfer coefficient of E_x generated by P_z dipole and M_y dipole can be expressed below, the other transfer coefficients can be similarly derived

$$T_{E_x\_P_z} = -j\frac{k_0\eta_0}{4\pi}\left[\frac{(z-h)(x-x')}{r_1^2}q_1(r_1) + \frac{(z+h)(x-x')}{r_2^2}q_1(r_2)\right] \tag{3.12}$$

$$T_{E_x\_M_y} = -j\frac{k_0^2\eta_0}{4\pi}\left[\frac{(z-h)}{r_1}q_3(r_1) + \frac{(z+h)}{r_2}q_3(r_2)\right] \tag{3.13}$$

A more general representation of the problem can be expressed as

$$Tx = F \tag{3.14}$$

Where T is the transfer matrix, x is unknown complex number that represents P_z, M_x and M_y. Normalization is also used to improve the matrix condition number and obtain a more accurate solution. Consider the magnetic field radiated by P_z, M_x and M_y dipoles,

$$\begin{bmatrix} [H_x]_{m\times 1} \\ [H_y]_{m\times 1} \end{bmatrix} = \begin{bmatrix} T_{Hx\_Pz} & T_{Hx\_Mx} & T_{Hx\_My} \\ T_{Hy\_Pz} & T_{Hy\_Mx} & T_{Hy\_My} \end{bmatrix} \begin{bmatrix} [P_z]_{n\times 1} \\ [M_x]_{n\times 1} \\ [M_y]_{n\times 1} \end{bmatrix} \tag{3.15}$$

First, the magnetic field data is normalized as

$$F_n = \begin{bmatrix} [H_x]_{m\times 1} / H_{\max} \\ [H_y]_{m\times 1} / H_{\max} \end{bmatrix} \tag{3.16}$$

In which $H_{\max}$ is the maximum magnitude of the tangential H fields. The equivalent dipole moments are also normalized as

$$X_n = \begin{bmatrix} [P_z]_{n\times 1} \\ [k_0 M_x]_{n\times 1} \\ [k_0 M_y]_{n\times 1} \end{bmatrix} \tag{3.17}$$

The normalized transfer matrix T_n are described as

$$T_n = \begin{bmatrix} T_{Hx\_Pz}/H_{\max} & T_{Hx\_Mx}/(H_{\max}k_0) & T_{Hx\_My}/(H_{\max}k_0) \\ T_{Hy\_Pz}/H_{\max} & T_{Hy\_Mx}/(H_{\max}k_0) & T_{Hy\_My}/(H_{\max}k_0) \end{bmatrix} \tag{3.18}$$

Using linear least-square method [14], the normalized solution X_n can be calculated as

$$X_n = [T_n' T_n]^{-1} T_n' F_n \tag{3.19}$$

3.2. NEAR FIELD MEASUREMENT

A passive board will be used to perform the RF interference study here as shown in Figure 3.1.The board size is 220mm × 160mm.The size of the patch antenna is 28mm × 37.2mm.A top view of the board model is shown in Figure 3.2.

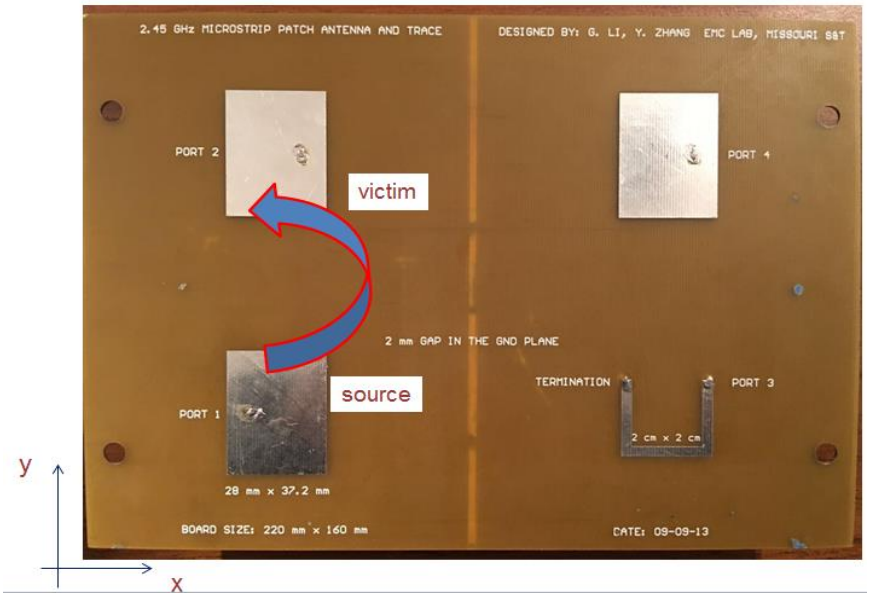

Figure 3.1. Patch antenna board for RFI study

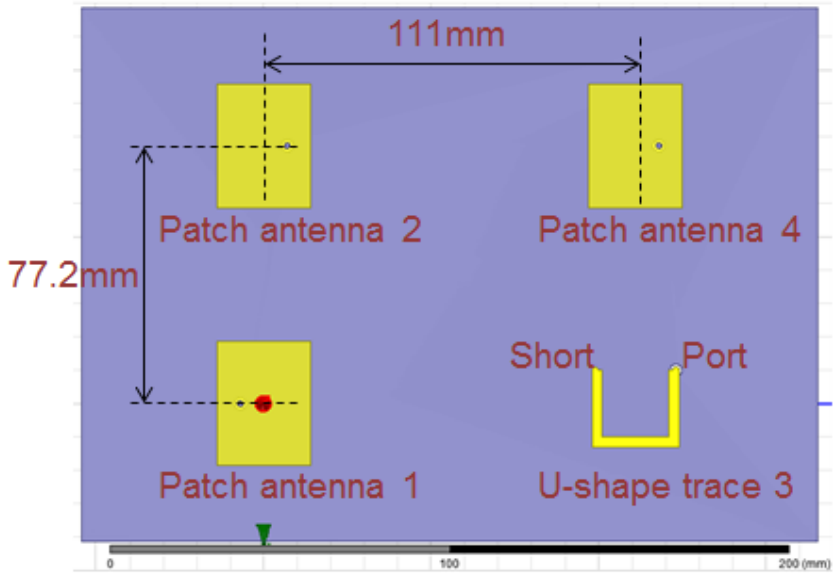

Figure 3.2. Top view of the board model

In real measurement, what the instruments measure is voltage. The relationship between the measured voltage and the real H field is built by probe factor. Probe factor is

calculated by measuring a simple 50 Ohm microstrip. The measured voltage of the 50 Ohm trace will be compared to field value in the simulation model. The measured voltage will be compared to simulation H field at different height. The probe factor can be calculated at the case when the pattern between measurement and simulation match the most [15] [16]. The setup for calibrating the H field probe is shown in Figure 3.3. The magnitude and phase of the probe factor are shown in 3.4.

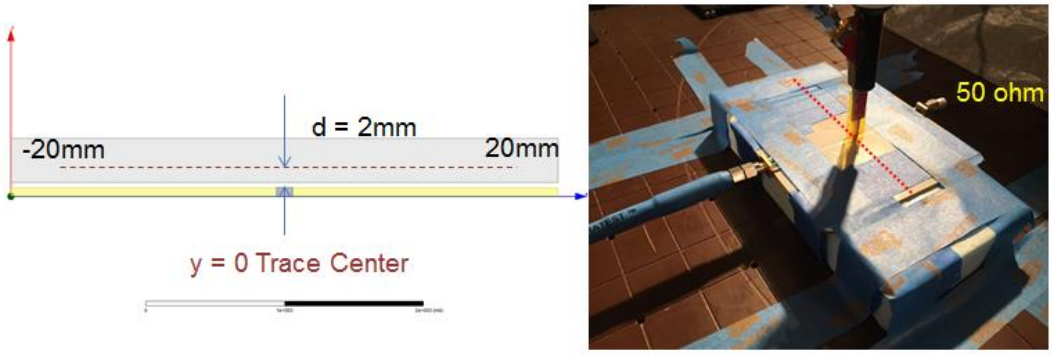

Figure 3.3. Calibration setup for H field probe

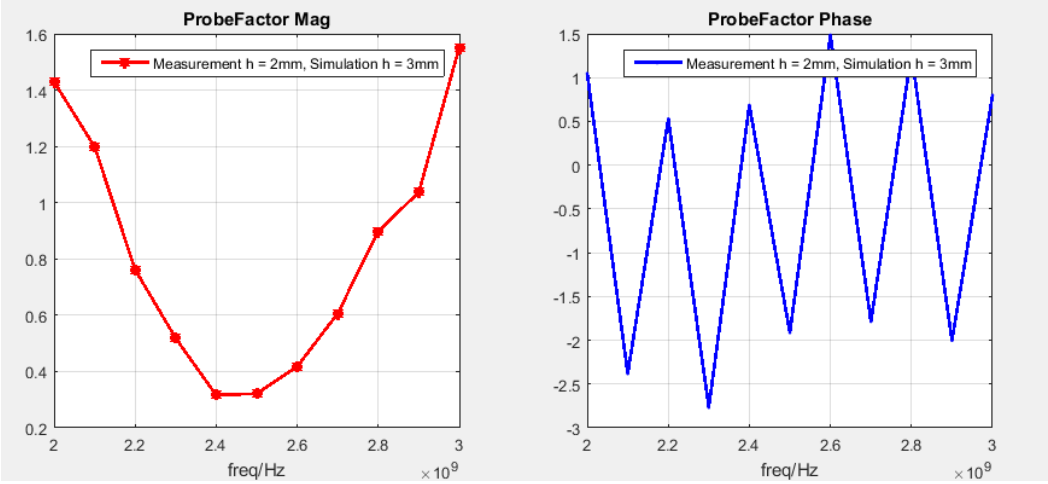

Figure 3.4. Probe factor of the H field probe

VNA S21 function is used to measure near field of the patch antenna which is a passive device. The measurement procedures are the same with the probe calibration. The measured tangential H field is shown in Figure 3.5.

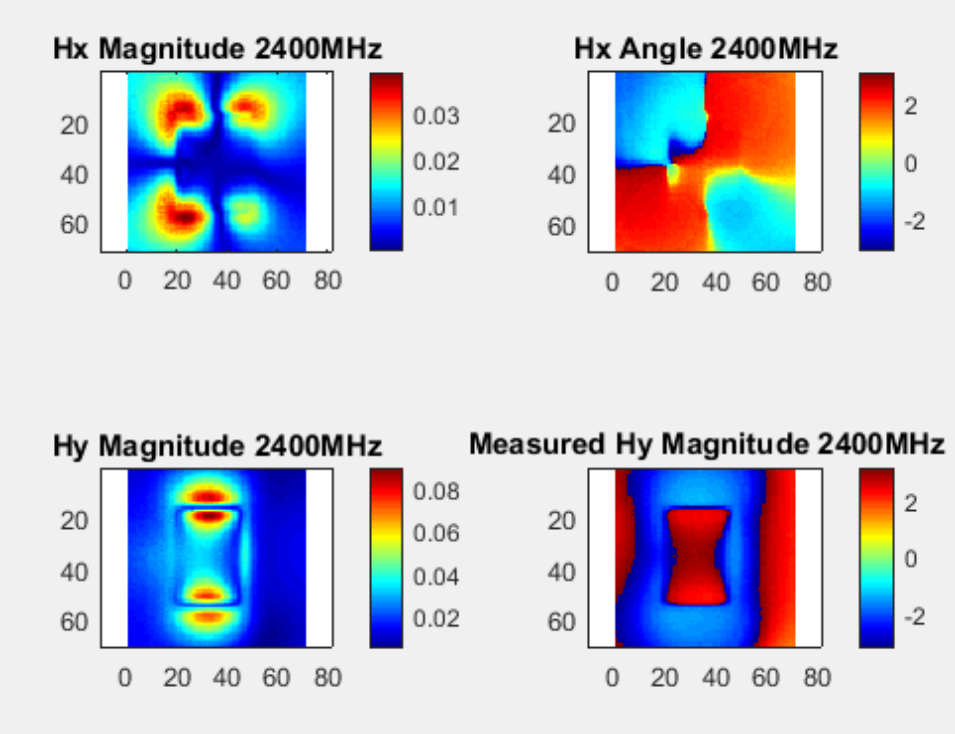

Figure 3.5. Measured H field data, 2mm above the patch

3.3. EQUIVALENT DIPOLE MOMENT MODEL

With tangential H field data, the unknown dipole moment can be solved based on the dipole sets as specified in Figure 3.6. This dipole set is predefined to be located at 8*8 locations. Pz, Mx and My will be put at those locations. The distance between each location is 9mm. All of the dipole moments are located 1mm above the ground plane. The way to select the dipole moment and where to place them is based on engineering experience. More studies will be done in the future to better guide the dipole selection.

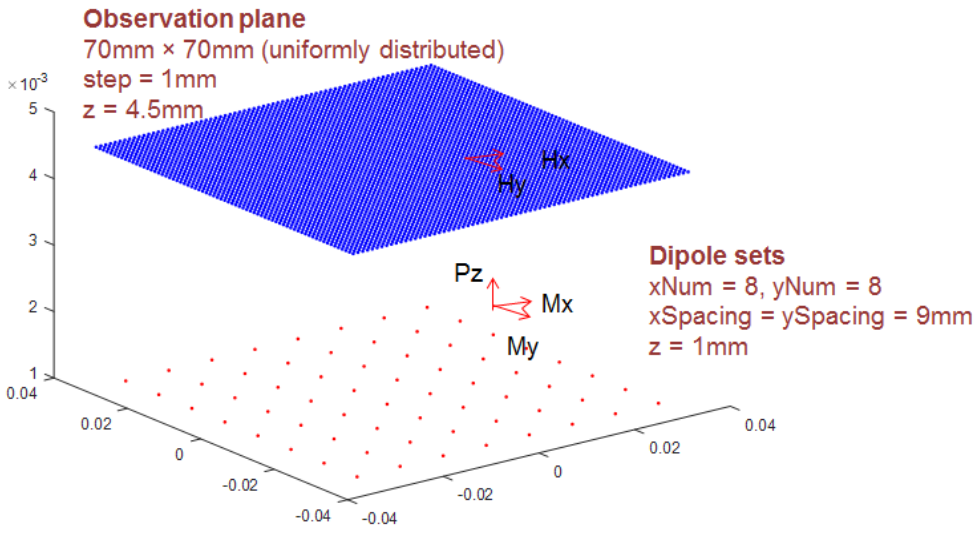

Figure 3.6. Location and type of the dipole set

Once the equivalent dipole moment model of the patch antenna is obtained, theoretically the field at anywhere can be calculated. Figure 3.7 shows the H field comparison between the measurement and the Matlab fitting. The fitted field shows a reasonable match with the measured field, although not perfect.

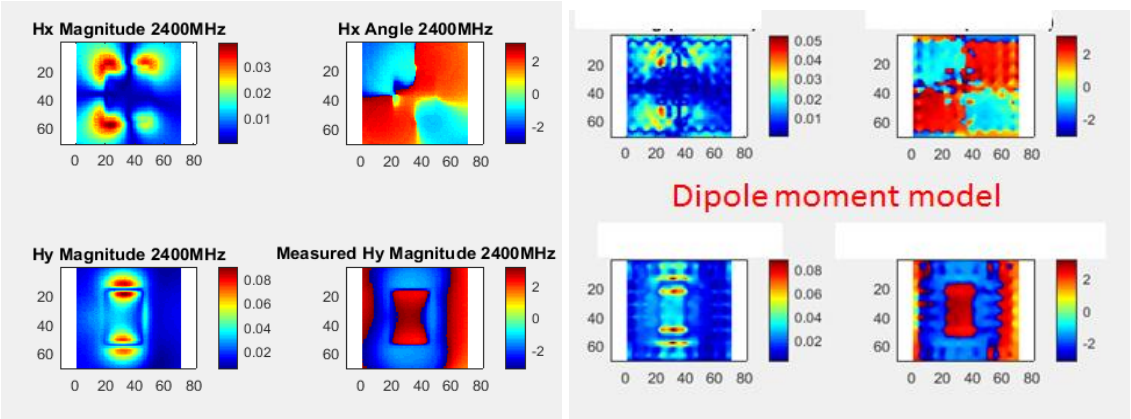

(a) (b)

Figure 3.7. H field at z=4.5mm,
from measurement (a) and from Matlab fitting (b)

The equivalent dipole moment model can also predict the field at z=10mm. Figure 3.8 shows the H field comparison between the measurement and the Matlab calculation at another observation plane. Reasonable match between the predicted field and measured field can be observed, at another observation z=10mm. The magnitude and phase of the dipoles are also shown in Figure 3.9.

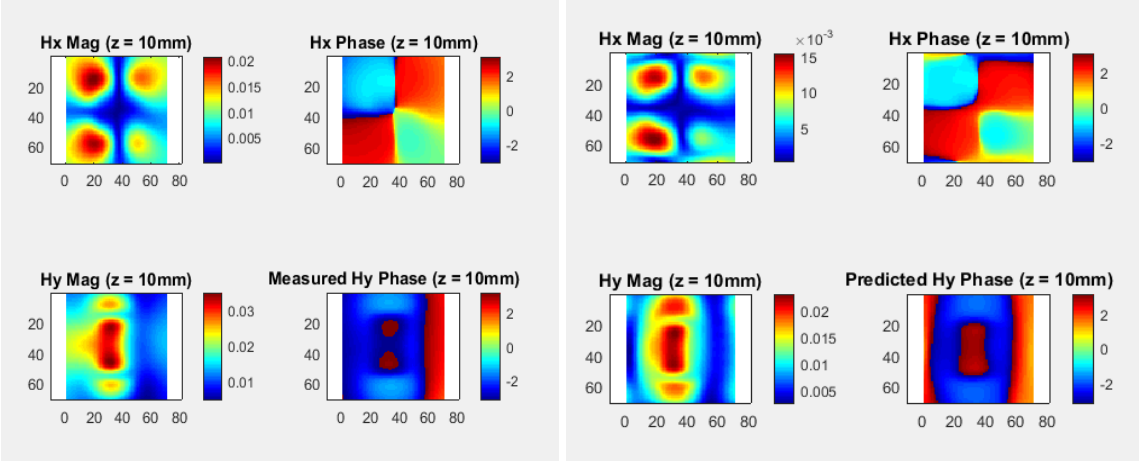

(a) (b)

Figure 3.8. H field at another plane z=10mm, from measurement (a) and from Matlab calculation (b)

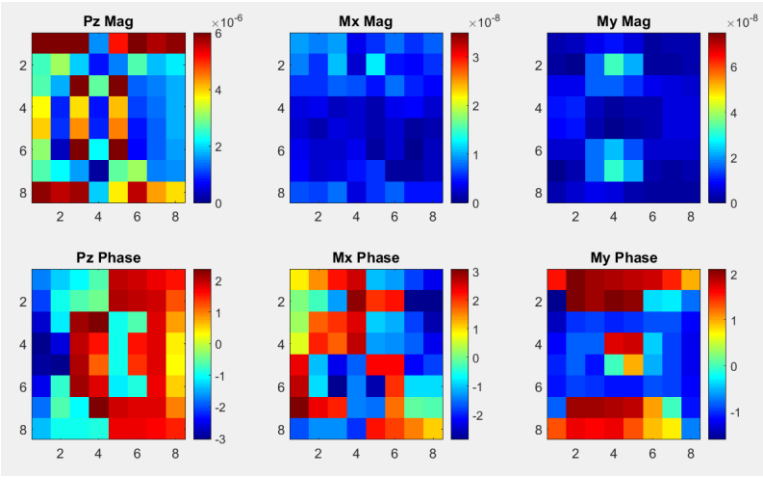

Figure 3.9. Magnitude and phase of the 8*8*3dipoles

3.4. COUPLED POWER VALIDATION

3.4.1. Coupled Power from Measurement. The setup of measuring coupled power is shown in Figure 3.10 (a) .The source patch antenna is excited by a 0dBm signal at 2.4GHz. Figure 3.10 (b) shows the coupled power is -35.0dBm.

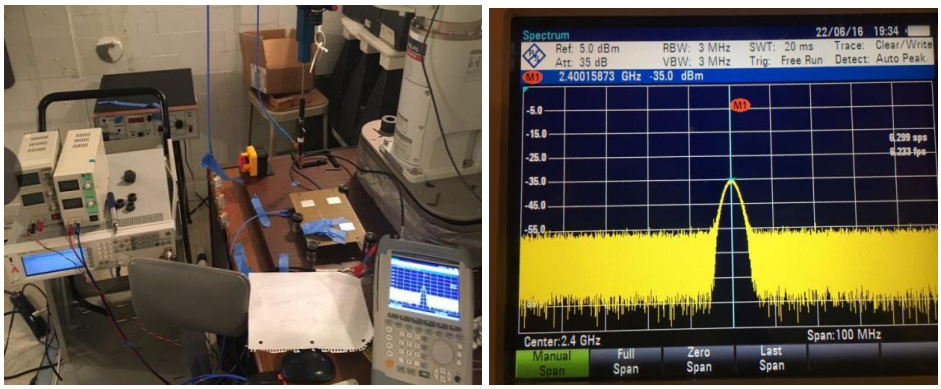

(a) (b)

Figure 3.10. Setup of measuring coupled power (a) and coupled power value (b)

3.4.2. Coupled Power from Equivalent Dipole Model. Import the dipole models into HFSS and draw the nearby antenna, as shown in Figure 3.11 (a).There are dipoles at 8*8 locations, while Pz ,Mx and My exist at each location, as shown in Figure 3.11 (b). So in total, there are 192 dipoles.

A 15 mm long coaxial cable is attached to the victim antenna to make sure TEM mode is obtained at the end of the coaxial cable. Two lines will be drawn from the inner connector of the coaxial cable to the outer ground of the connector as shown in Figure 3.12.

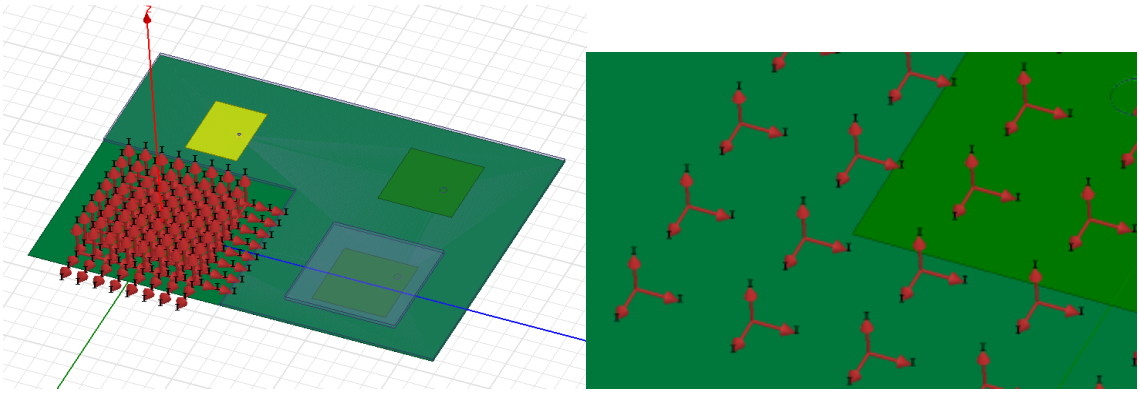

(a) (b)

Figure 3.11. Equivalent dipole moment model in HFSS (a) dipole details (b)

Since only TEM mode exists at the end of the coaxial cable, integral along two different lines will yield the same voltage. The voltages from these two lines are 0.00427 V, 0.00434 V. The difference of these two voltages is small enough. Based on the coupled voltage, the coupled can also be calculated as -37.39 dBm. Previous measurement shows that the coupled power is -35 dBm. The difference between the dipole moment estimation and the direct measurement is less than 3dB, which is good enough for most engineering application.

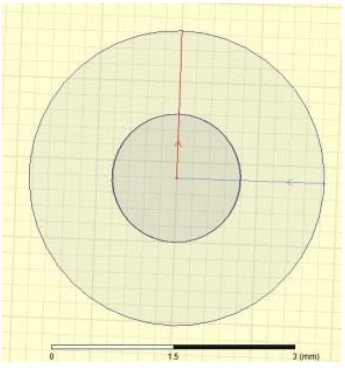

Figure 3.12. E field integral to get the coupled voltage

Figure 3.13 shows the E field at the end of the coaxial cable. Clearly tangential E field exist, while normal E field in nearly 0, which is the property of the TEM mode.

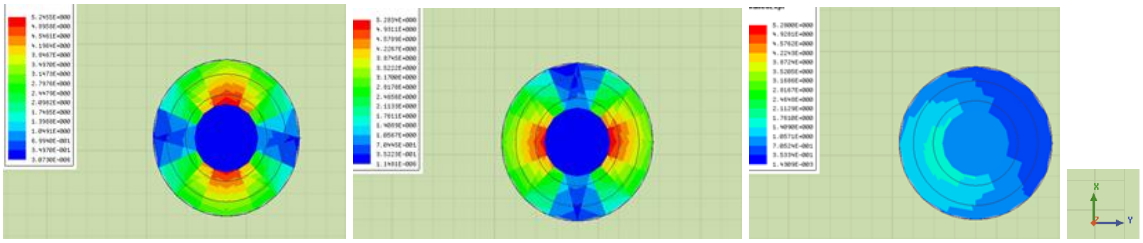

Figure 3.13 Ex (a), Ey (b), Ez (c) magnitude plot at the end of the coaxial cable

Another validation to demonstrate the correctness of the simulation is shown in Figure 3.14. E field comparison between the Matlab calculation and HFSS simulation also shows good match.

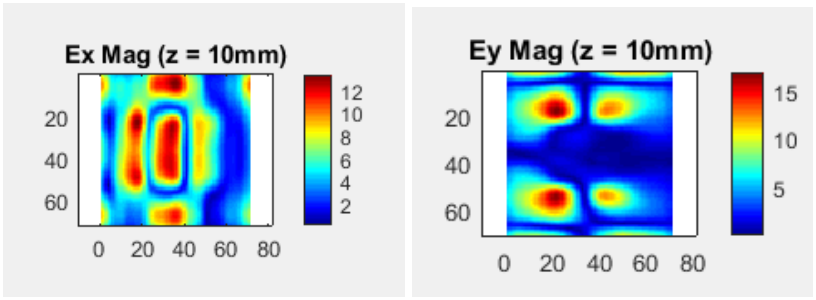

(a)

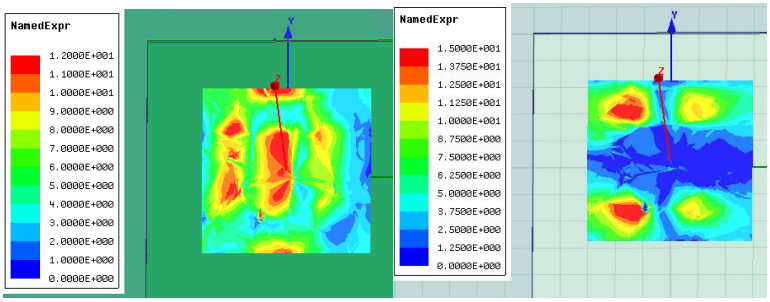

(b)

Figure 3.14 Tangential E field from Matlab (a) and HFSS simulation (b)

4. CONCLUSIONS

For the impedance measurement of the clips, considering the practical application of the O Clip, a de-embedding method is proposed to measure the impedance measurement of the connector in the frequency range up to 20 GHz. The de-embedding results are verified by simulation results and also measurement results. One thing worth to point out is that although only O and C clips are measured in this study, other small components can also be measured using the same method, for example conductive foam, which is also widely used in cellphone industry.

Also, the equivalent dipole moment model is studied for RFI estimation. Future work include: reduce the errors, reduce the simulation time [17] [19]. Currently, there are no clear guidelines for how many dipoles to choose, where to place them. A clear guideline can be established in the future to guide users to use this method. Simulation time is also another problem; currently each frequency point needs a separate simulation which costs 10s of hours sometimes. More time-reducing approaches need to be applied here [20][23].

BIBLIOGRAPHY

[1] H.B Ye, W.Wu, J.Zhou. "Innovative O-shape spring contact used in mobile device." In *Electromagnetic Compatibility (EMC), 2013 IEEE International Symposium on*, pp. 779-782. IEEE, 2013.

[2] T.Yonekura, M.Jansons."High frequency impedance analyzer." *CARTS-EUROPE 1993 proceedings*, pp. 44-52.

[3] N.Erickson, K. Shringarpure, J. Fan, B. Achkir, S.Pan, Chulsoon Hwang, "De-embedding techniques for transmission lines: an exploration, review and proposal." In *Electromagnetic Compatibility (EMC), 2013 IEEE International Symposium on*, pp. 840-845. IEEE, 2013.

[4] Agilent Technologies, "A simple, power method to characterize differential interconnects.", Jun.2012.

[5] David.M.Pozer. "Microwave Engineering." 3rd Edition,wiley, Dec. 2012.

[6] Li, Liang, Jingnan Pan, Chulsoon Hwang, Gyuyeong Cho, Harkbyeong Park, Yaojiang Zhang, and Jun Fan. "Measurement validation for radio-frequency interference estimation by reciprocity theorem." In *Electromagnetic Compatibility (EMC), 2015 IEEE International Symposium on*, pp. 154-159. IEEE, 2015.

[7] Li, Liang, Jingnan Pan, Chulsoon Hwang, Gyuyeong Cho, Harkbyeong Park, Yaojiang Zhang, and Jun Fan. "Near-field coupling estimation by source reconstruction and Huygens's equivalence principle." In *Electromagnetic Compatibility and Signal Integrity, 2015 IEEE Symposium on*, pp. 324-329. IEEE, 2015.

[8] Li, Liang, Jingnan Pan, Chulsoon Hwang, Gyuyeong Cho, Harkbyeong Park, Yaojiang Zhang, and Jun Fan. " Radio-Frequency Interference Estimation by Reciprocity Theorem with Noise Source Characterized by Huygens's Equivalent Source." Accepted to be published in *Electromagnetic Compatibility and Signal Integrity, 2016 IEEE Symposium on.*

[9] Li, Liang, Jingnan Pan, Chulsoon Hwang, Gyuyeong Cho, Harkbyeong Park, and Jun Fan. "Application of Reciprocity Theorem in Radio Frequency Interference Estimation." Accepted to be published in *Electromagnetic Compatibility and Signal Integrity, 2016 Asia-Pacific International Symposium on.*

[10] Wilson, P. "On correlating TEM cell and OATS emission measurements."*Electromagnetic Compatibility, IEEE Transactions on* 37, no. 1 (1995): 1-16.

[11] Yu, Zhenwei, Jason A. Mix, Soji Sajuyigbe, Kevin P. Slattery, and Jun Fan. "An improved dipole-moment model based on near-field scanning for characterizing near-field coupling and far-field radiation from an IC."*Electromagnetic Compatibility, IEEE Transactions on* 55, no. 1 (2013): 97-108.

[12] Yu, Zhenwei, Jayong Koo, Jason A. Mix, Kevin Slattery, and Jun Fan. "Extracting physical IC models using near-field scanning." In *Electromagnetic Compatibility (EMC), 2010 IEEE International Symposium on*, pp. 317-320. IEEE, 2010.

[13] Balanis, Constantine A. *Antenna theory: analysis and design*. John Wiley & Sons, 2016.

[14] Strang, Gilbert. *Introduction to linear algebra*. Vol. 3. Wellesley, MA: Wellesley-Cambridge Press, 1993.

[15] Zhang, Ji, Keong W. Kam, Jin Min, Victor V. Khilkevich, David Pommerenke, and Jun Fan. "An effective method of probe calibration in phase-resolved near-field scanning for EMI application." *Instrumentation and Measurement, IEEE Transactions on* 62, no. 3 (2013): 648-658.

[16] T. Li, V. Khilkevich and D. Pommerenke, "Phase-Resolved Near-Field Scan Over Random Fields," in *IEEE Transactions on Electromagnetic Compatibility*, vol. 58, no. 2, pp. 506-511, April 2016.

[17] Tong, Xin, D. W. P. Thomas, A. Nothofer, P. Sewell, and C. Christopoulos. "A genetic algorithm based method for modeling equivalent emission sources of printed circuits from near-field measurements." In 2010 Asia-Pacific International Symposium on Electromagnetic Compatibility. 2010.

[18] Tong, Xin. "Simplified equivalent modelling of electromagnetic emissions from printed circuit boards." PhD diss., University of Nottingham, 2010.

[19] CST – Computer Simulation Technology. [Online]. Available: https://www.cst.com/ May 7, 2016.

[20] J. Pan, L. Li, X. Gao and J. Fan, "Application of dipole-moment model in EMI estimation." *2015 IEEE International Symposium on Electromagnetic Compatibility and EMC Europe*, Dresden, 2015, pp. 350-354.

[21] J. Pan, X. Gao and J. Fan, "Far-field prediction by only magnetic near fields on a simplified Huygens's surface." *IEEE Trans. Electromagn. Compat.*, vol. 57, no. 4, pp. 693-701, Aug. 2015.

[22] J. Pan, H. Wang, X. Gao, C. Hwang, E. Song, H. Park and J. Fan, "Radio-frequency interference estimation using equivalent dipole-moment models and decomposition method based on reciprocity. " *IEEE Trans. Electromagn. Compat.* vol. 58, no. 1, pp. 75-84, Feb. 2016.

[23] J. Pan, X. Gao, Y. Zhang, J. Fan, "Far-field radiation estimation from near-field measurements and image theory." in *Proc*. *IEEE International Symposium on Electromagnetic Compatibility.*, Raleigh, NC, Aug. 2014, pp. 609-614.

VITA

Qiaolei Huang was born in Hanchuan, Hubei, China. He received his B.S. degree in Electronics and Information Engineering from Huazhong University of Science and Technology, Wuhan, China, in 2013. He joined the EMC Laboratory in the Missouri University of Science and Technology, Rolla, in 2013 and received the M.S. degree of Electrical Engineering in December 2016. He worked as a Co-op Engineer at Cisco EMC Design Team and OTA test team in 2015.

His research interests included signal integrity, radio-frequency interference, near field scanning technology.